Contents

ACKNOWLEDGEMENTS

I would like to express my deep gratitude to the following people for the help received throughout the project: Dr Stuart Haigh and Dr April Bowman, my research supervisors, for their patient guidance, encouragement and useful critiques of this research work; Geoff Eichhorn and Chuhan Deng, PhD research students, for their advice and assistance in setting up the experiment. Finally, I would also like to thank the staff and technicians in the Schofield Centre who helped to assemble the lab equipment and assisted in laboratory work.

NOMENCLATURE

APT	Accelerated Pavement Test
PIV	Particle Image Velocimetry
w	Vertical deflection
ϵ_t	Horizontal strain
σ_z	Vertical stress
σ_r	Radial stress
σ_t	Horizontal stress
τ_{rz}	Shear stress
q	Pressure
a	Radius of circle
z	Depth of layer
σ_{Is}	Standard deviation of subset pixel intensities
SSSIG	Sum of square of subset intensity gradients
P	Load applied
n	Number of cycles
v	Speed of wheel
Q	Volumetric flow rate
R	Radius of wet region
γ	Shear strain
ϵ_v	Volumetric shear strain
ν	Poisson's ratio
E	Young's modulus

1 INTRODUCTION

1.1 Background

Road infrastructure is the most important of all public assets. Road networks greatly contribute to the nation's economic development and growth. They provide access to employment, social, health and education services. In the UK alone, the road network totals to about 422,100 km of paved roads.

In Cambridgeshire, as in the rest of the UK, road conditions have worsened over recent years, as indicated by the increasing number of potholes due to the cold and wet weather. These potholes have a great impact on Cambridgeshire Council and Central Government expenditure, with £2.9 million being spent on resurfacing roads and pothole repairs in 2017 alone. According to data gathered by the RAC (a British automotive services company) in a freedom of information request (FOI) to councils, Cambridgeshire saw a 124% increase in the number of potholes reported, from 2,236 potholes in 2015 to 5,018 in 2017 (Leishman, 2019). The chances of a pothole forming significantly increase during the winter months.

Potholes are a safety hazard. Hitting a pothole can cause damage to a vehicle's wheels and suspension. It can lead to accidents as vehicles become less stable and manoeuverable. Potholes also have an impact on the country's economy as there will be an increase in vehicle, insurance and maintenance costs and travel time. The typical repair mechanism of potholes in Cambridge is the use of a machine known as the Dragon Patcher. The 'dragon' fires flames to dry out the road surface, which is then cleaned with compressed air and sealed with a stone mix and hot bitumen. However, the weak subgrade layer which is moisture sensitive is never treated, resulting in the reoccurrence of potholes over the same spot.

1.2 Pavement failure

A typical road consists of four different layers: surface course, binder course, base layer and subgrade, each with varying thicknesses, such as the one shown in Figure 1. Pavement structures are designed to distribute traffic induced stresses and strains over the load-bearing layers in order to provide structural adequacy over the pavement's design life. The surface course is the layer that comes in contact with traffic, while the binder course is the load-bearing, strengthening layer of the pavement. The base layer provides additional load distribution and allows drainage of water. Finally, the subgrade is the in situ material upon which the pavement structure is placed.

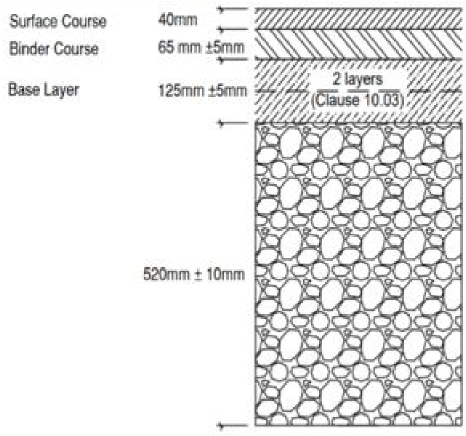

Figure 1: Typical pavement in Cambridge

Previous research has shown that about 30% to 70% of surface rutting occurs in the subgrade (Qiao, 2014). However, most research and repair work have only focused on the surface layer and there is little understanding of the subgrade failure, which is instrumental to the development of potholes.

Two of the main causes of subgrade failure are traffic loading and water ingress. An increase in loading magnitude and number of load repitition affect the performance of pavements as the subgrade becomes weaker in supporting wheel loads. Infiltration of water further reduces the support strength of the granular subgrade, as the layer experiences loss of particles interlock and subsequent particle displacement, which eventually leads to subgrade failure and formation of potholes. Excess water in a pavement structure can decrease its life by more than half (Cedergren, 1988). This process can happen over the course of days, months or even years in some cases, but can be prevented with crack repair. Besides water causing the loss of strength in subgrade, in extreme cold weather, water that seeps through existing cracks in the road can freeze and expand. Over time, the water melts and eventually evaporates or drains into the surface, creating a 'gap' underneath the road's surface, which is broken through by the traffic. Hence, a pothole is formed. Figure 2 shows the conceptual pavement stiffness variations due to freezing and thawing. There is a significant weakening of structure once the winter season is over.

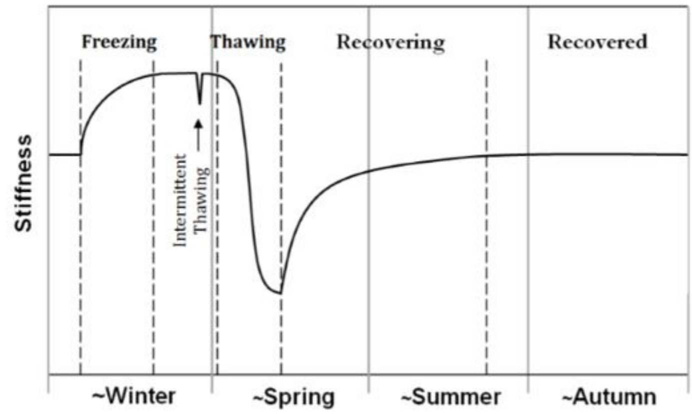

Figure 2: Conceptual pavement stiffness variations due to freezing and thawing (Salour, 2015)

The moisture condition in pavements and its impact on the structural performance have been of great interest among pavement researchers. A proper understanding of the impact of water on the subgrade layer is important for future mechanistic pavement design.

1.3 Aims & objectives

The main aim of this research project was to provide more insight into the influence of water on the structural behaviour of subgrade through laboratory experiments. The specific objectives of the study were as follows:

- To replicate a typical pavement in the Accelerated Pavement Test (APT)
- To study the impact of water infiltration on the subgrade as surface loads and cycles increase
- To investigate the influence of thickness of base course on the deformation of the subgrade layer

It is important to note that the results from this project were only applicable to sandy regions. The project also tended to focus on the short-term response of the subgrade.

2 LITERATURE REVIEW

2.1 Accelerated pavement testing & influence of water on pavements

Pavement failure is observed when the surface asphalt layer develops cracks and ruts which lead to decreasing serviceability as the permanent deformation worsens. Accelerated load testing of pavements was done with the HVS-NORDIC at VTI in Sweden in 1998 (Wiman, 2001) to investigate pavement response and pavement performance. Figure 3 shows the rut depth measurements obtained by Wiman.

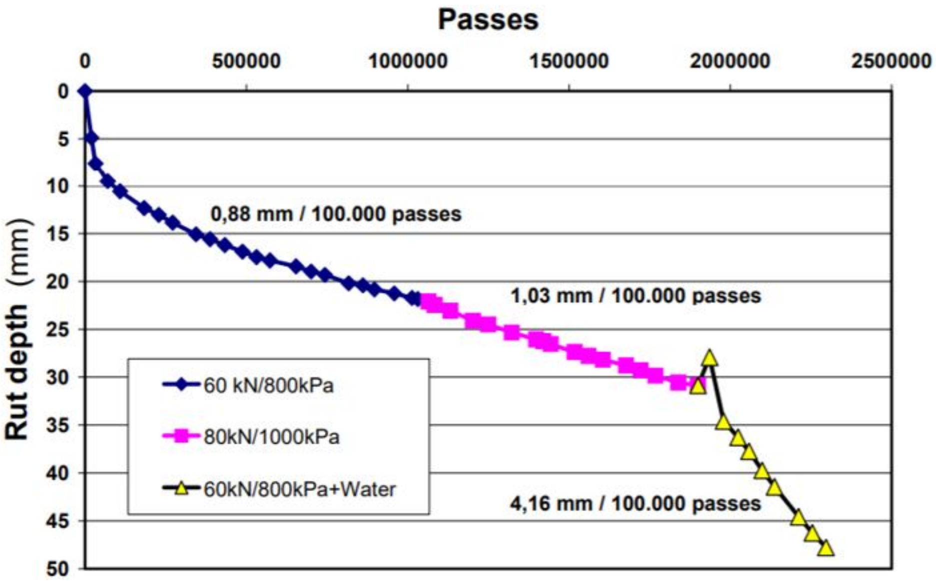

Figure 3: Rut depth measurements with increasing passes (Wiman, 2001)

It can be seen that with a 60 kN load, after 500,000 passes, the increase in rut depth was constant at 0.88 mm/100,000 passes. As the test load was increased from 60 kN to 80 kN, the rut propagation rate increased but only slightly to a rate of 1.03 mm/100,000 passes. Water was then introduced into the sand to the level 300 mm below the surface of the subgrade to weaken it. At a test load of 60 kN, the rut propagation increased markedly to 4.16 mm/100,000 passes and the first cracks were observed at the surface. The research conducted by Wiman has shown that water has a substantial impact on the pavement failure. However, the focus was only on the rutting surface and there was little understanding on the failure of the layers underneath it.

Erlingsson (2010) performed a study based on Accelerated Pavement Testing (APT) of an instrumented thin flexible pavement to investigate the influence of the moisture content on the performance of the pavement structure. 500,000 of the load passages were conducted while the pavement structure was in its natural moisture condition and 500,000 load passages were conducted after the groundwater table was raised to 30 cm below the top of the subbase. From the measurements and the numerical analyses of the data, it was observed that introducing water into the system resulted in larger permanent and resilient strains in all the unbound layers. In similar studies by Saevarsdottir & Erlingsson (2013a), all the unbound layers showed increased permanent and resilient deformations as the moisture content increased, with the most dramatic increase in the subgrade layer.

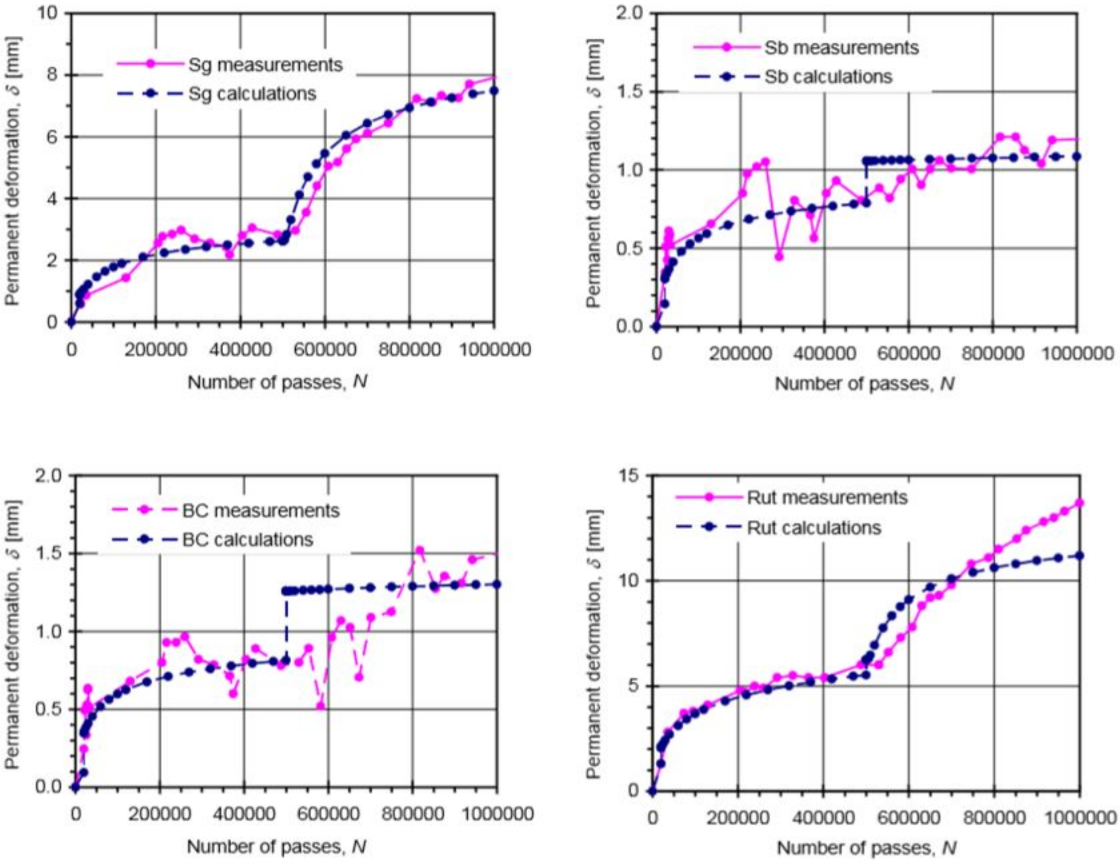

Figure 4: Permanent deformation development as a function of the number of load repetitions. $W = 60kN$ and tyre pressure $= 800kPa$. $Sg = subgrade$, $Sb = subbase$ and $BC = basecourse$. One million load cycles are shown. Water was pumped after 500,000 repetition. (Erlingsson, 2010)

Based on Figure 4, the largest influence of the groundwater table was in the sandy subgrade. Both the subbase and the base course were much coarser and therefore had a much lower ability to attract water. This explains why they were not affected to the same extent as the subgrade. Erlingsson introduced water into the soil by raising or lowering the groundwater table. This was different from modelling rainwater whereby water seeps into the ground at a rate depending on the rainfall intensity. Also, similar to Wiman's accelerated load test, the failure mechanism in the subgrade was not exactly known.

Unbound granular materials and subgrade soils significantly contribute to the overall bearing capacity of pavement structures. In fine-grained materials and subgrade soils, pore water usually affects the effective stress of the soil structure due to a decrease in pore suction which will result in reduction in material stiffness and strength. In coarse-grained granular materials (such as the limestone aggregates used in this project), an increase in moisture content can result in reduction in the resilient modulus due to decreased contact friction and particle interlock strength (Lekarp et al., 2000; Ekblad & Isacsson, 2006). Gaspard, et al. (2019) showed that an increase in moisture content above the optimum level significantly reduces the resilient modulus of the soil, resulting in loss of soil strength and faster pavement failure.

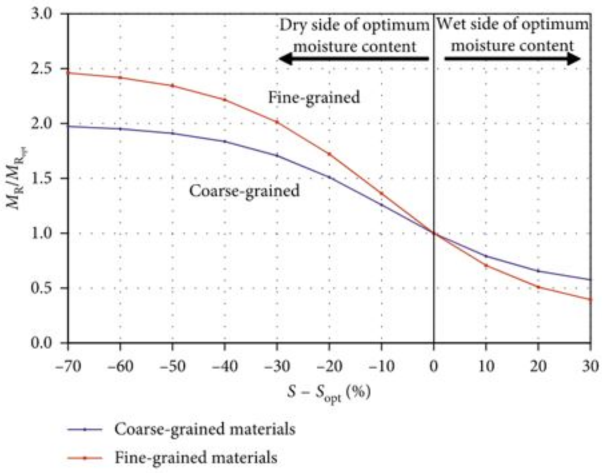

Figure 5: Effect of moisture changes on resilient modulus (Gaspard, et al., 2019)

Resilient modulus of subgrade soils is the primary material property for design and analysis of pavements. Seasonal variation of subgrade moisture content can significantly affect subgrade resilient modulus and subsequently pavement design. Haynes & Yoder (1963) reported on the behaviour of granular materials in pavements and susceptibility to water. Figure 6 shows their study on the deformation and resilient (rebound) response of gravel and crushed stone. For the test on crushed stone, between approximately 60% and 80% degree of saturation, the resilient deformation increased by about one third. As for the gravel, at a saturation level of almost 98%, the resilient deformation doubled compared to that at the saturation level of 70%.

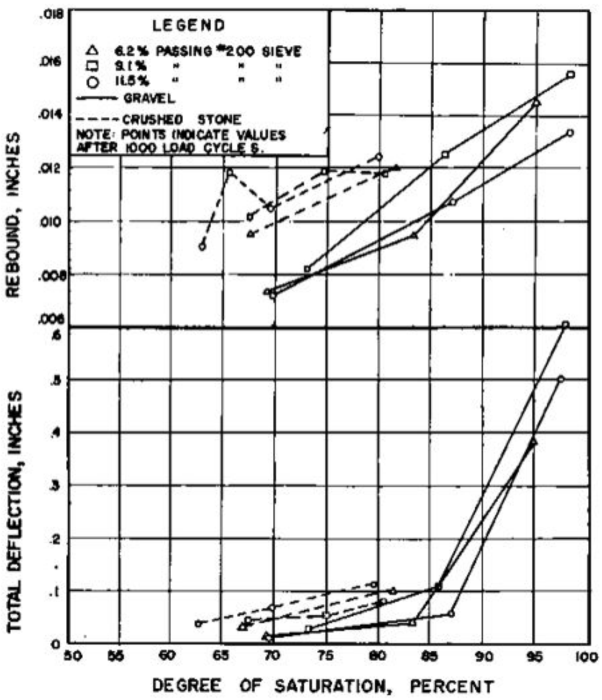

Figure 6: Deflection and resilient response of gravel and crushed stone at different saturation level (Haynes & Yoder, 1963)

2.2 Influence of base course thickness on deformation

Bowman & Haigh (2018) also carried out a study based on APT. It was found that the displacement spread wider in each subsequent layer with a thinner base course. On the other hand, the displacement in the test with a thicker base course was more localised to the area directly beneath the tyre. It was also observed that using laser surface scanning, the layer thickness altered the deformation behaviour of the surface beneath the tyre (Figure 7). With a thicker base and subbase, rutting progressed linearly as the number of load applications increased, suggesting steady plastic movement of the subsurface material. With the thinner base and subbase, deformation increased in a non-linear fashion, suggesting plastic, progressive failure.

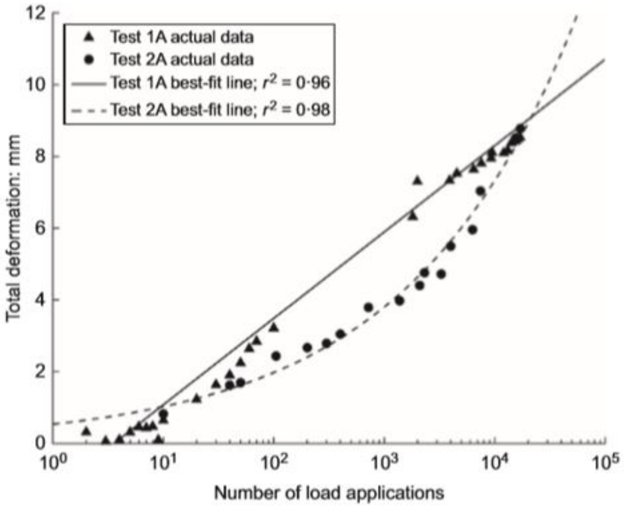

Figure 7: Measured and predicted surface deformation under tyre as a function of number of cycles. Test 1A-220 mm base and 100 mm subbase. Test 2A-40 mm base and 40 mm subbase. (Bowman & Haigh, 2018)

Nazeri et al., (2018) investigated the effect of thickness of base course on load-settlement characteristics of sandy subgrade using plate load test. The settlement in the weak subgrade without base application was a lot higher than the settlement in the presence of base course. It was found that the settlement decreased as the thickness of the base course increased (Figure 8). However, the test only considered static load and was performed close to the optimum moisture level.

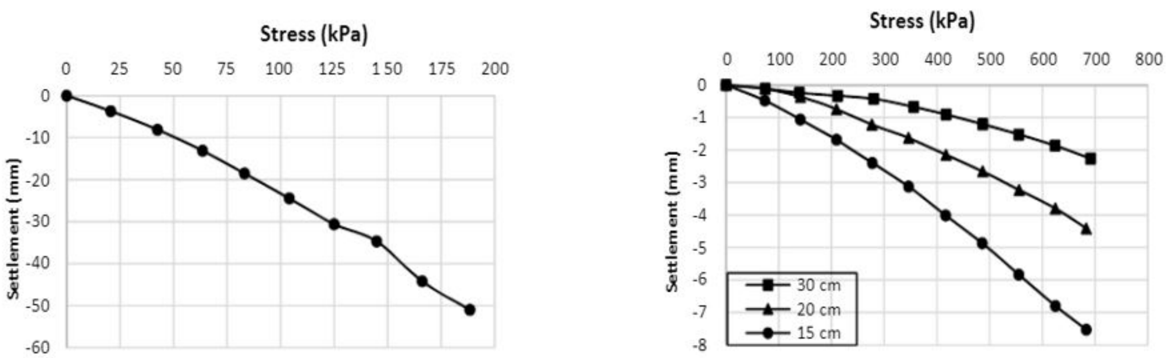

Figure 8: Stress-settlement curves of sandy subgrade in loose condition (left), and application of base course in different thicknesses (right) (Nazeri et al., 2018)

2.3 Analytical models for deformation and stress in pavements

The stress, strain and deformation in a pavement can be predicted using different analytical models under simulated wheel and environmental loading conditions. The main models are based on multilayer elastic theory and finite element analysis.

Finite element analysis

Saad (2014) conducted a coupled finite element (FE) study to investigate the mechanical response of a flexible pavement under various excess moisture conditions of its granular foundations. In saturated foundations, there was a remarkable increase of surface deflection, Δw and horizontal strain, ϵ_t in the vicinity of the wheel. The coupled non-linear FE analyses carried out on the conventional flexible pavement system showed that $(\Delta w)_{max}$ and $(\epsilon_t)_{max}$ increased by 287% and 191%, respectively, when the subgrade became fully saturated. The corresponding increases of $(\Delta w)_{max}$ and $(\epsilon_t)_{max}$ reached 459% and 264% when the pavement was subjected to the extreme moisture state of fully saturated base and subgrade.

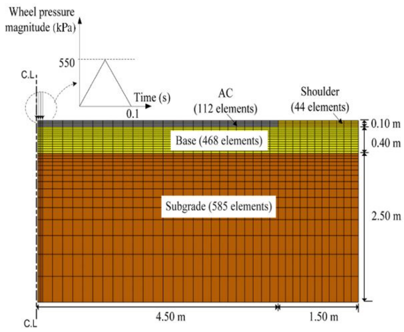

Figure 9: Finite element modelling on flexible pavement (Saad, 2014)

One-layer system

Foster and Ahlvin (1954) developed charts for computing vertical, tangential and radial stresses. The charts were developed for a Poisson's ratio of 0.5. Due to the axis of symmetry, only three normal stresses are considered, σ_z, σ_r and σ_t and one shear stress τ_{rz}. The load is not a point load, but distributed over an elliptical area. Therefore, the contact area can be approximated to a circular shape. If one-layer system is assumed as a homogeneous half space, Boussinesq equations can be applied. Boussinesq equations were developed for computing stresses in a homogeneous, isotropic and elastic media due to a point load at the surface. Assuming the tyre is a uniformly loaded round circle, the vertical compressive stress and deformation can be calculated with equations 1 and 2.

$$\sigma_z = q\Big[1 - \frac{z^3}{(a^2 + z^2)^{1.5}}\Big] \tag{1}$$

$$w = \frac{(1+\upsilon)qa}{E}\Big[\frac{a}{(a^2+z^2)^{0.5}} + \frac{1-2\upsilon}{a}[(a^2+z^2)^{0.5} - z]\Big] \tag{2}$$

where q is pressure, a is radius and z is depth.

Two-layer system

The effect of layers above the subgrade is to reduce the stress and deflections in the subgrade. Various multilayer theories for estimating stresses and deflections have been proposed. However, Burmister (1958) proposed basic theories that utilize assumptions close to actual conditions in a flexible pavement. Burmister obtained solutions for two-layer problems using strain continuity equations. Vertical stress decreases with an increase in modular ratio (i.e., E_1/E_2). Figure 10 shows the vertical stress patterns in two-layer systems.

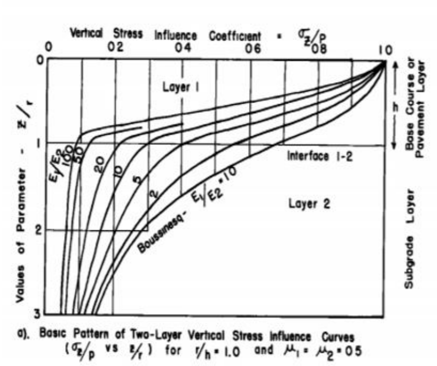

Figure 10: Two-layer vertical stress patterns (Burmister, 1958)

To summarise, most laboratory investigations reported a loss in resilient modulus when the moisture content in soil was increased. However, the deformation and failure of pavements were mainly focused on the surface asphalt layer despite studies showing subgrade failure as the main cause of pavement failure. Therefore, more study is required to better understand the behaviour of subgrade layer under moving wheel loads. Analytical models based on multilayer elastic theory and finite element analysis can be used to predict the stress, strain and deformation in the subgrade layer.

3 EXPERIMENTAL SETUP & METHODOLOGY

3.1 Materials selection

Two groups of soils were used in this project: Oxford sand (imported from Kazakhstan) as the subgrade and limestone aggregates as the base course. Oxford sand was chosen as it provided a natural variation in silt content while maintaining consistent sand gradation and limited organic content. Table 1 shows the properties of the two soils.

Table 1: Properties of soils

Type of soil	Mean particle size, D_{50} (mm)	Maximum voids ratio	Specific gravity	Optimum moisture content (%)	Dry unit weight (kN/m^3)
Oxford sand (subgrade)	0.21	0.77	2.65	11.1	18.00
Limestone aggregates (base course)	1.48	5.60	N/A	12.8	16.08

3.2 Installation of Perspex window

A transparent 100 mm thick Perspex (also known as PMMA) window was mounted inside a concrete tank that was 1.0 m deep but filled with Oxford sand up to a depth of 0.50 m, 0.86 m long and 0.80 m wide. The window was placed 18 cm away from one side of the wall (as shown in Figure 11), so that the wheel path was not blocked when the APT was put in place.

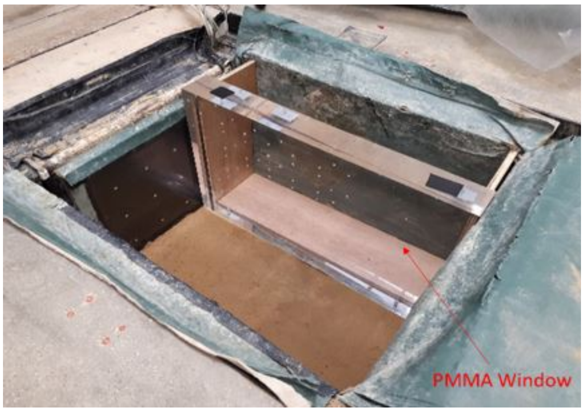

Figure 11: Installed perspex window

Control points (black dots with white background) were marked on the Perspex window as shown in Figure 12. These fixed points of known coordinates allowed calibration of location of the test patches (further explained in Section 3.8) when performing PIV analysis and were useful to stitch images from different cameras together.

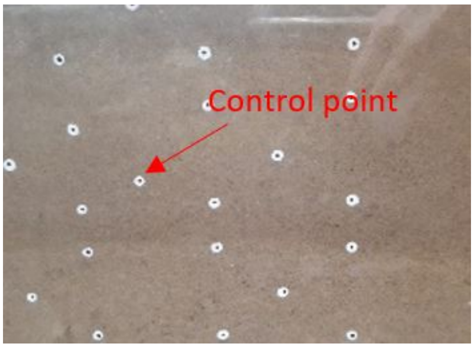

Figure 12: Control point on window

When the first few tests without the base course were conducted, it was found that rutting caused the sand to build up in the gap between the window and the tyre. The wider the gap, the more the rut that built up within the gap. This made it difficult to identify the position of the tyre in the images captured by the cameras. The length of the gap was measured and was reduced to a width of 1 cm by moving the window further away from the wall by another 2 cm. The pavement was removed from the concrete tank, so that the window could be moved closer to the wheel.

3.3 Installation of cameras

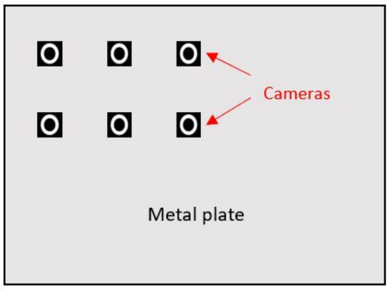

Figure 13: Layout of cameras

A metal plate about 1cm thick was coated with anti-reflection black paint. Holes were drilled onto the plate and six cameras were mounted on it. The Raspberry Pi cameras used were capable of capturing 3280×2464 pixel images. The layout of the cameras is shown in Figure 13. The six cameras were placed in a way that there was overlapping of images. The metal plate was then placed against the wall behind the window. The cameras were set to capture images of the soil movement at intervals of 1 second when running the experiment.

Object illumination and texture of the soil greatly influence the quality of images which will then affect the results of PIV. Therefore, the window was cleaned and LED lights were placed on top of the window to give homogenous and consistent lighting. A lens adjustment tool was simply placed over the camera lens - set nicely without force, and then turned left or right to adjust the focus until a sharp image was obtained.

3.4 Compaction of soil

Once the window was inserted, the soil was compacted in layers to form the pavement. The procedures for the compaction of soil were as follows:

1. The water content of the soil was first measured by obtaining a small sample in a cup and putting it in the oven at 100°C for at least 24 hours. The dry sample was weighed and the water content was given by $\frac{Mass of water(g)}{Mass of solid(g)} \times 100\%$.

2. If the water content of the soil was lower than the optimum water content, water was then added to the soil in a mixer. The mixer was left running for at least 15 minutes to allow even mixing of water and soil.

3. The soil was emptied into the concrete tank by tilting the mixer and running it at the same time.

4. The soil was levelled by hand using a leveller. Once it was levelled, the soil was compacted with a vibrator to its optimum Proctor value. Each soil layer has to be within a thickness of 150 mm to ensure good compaction.

5. Steps 1 to 4 were repeated until the soil was almost at the same level as the top of the Perspex window.

Once the pavement was levelled and compacted, the accelerated pavement tester (APT) was bolted in place with the help of the technicians.

3.5 Accelerated Pavement Tester (APT)

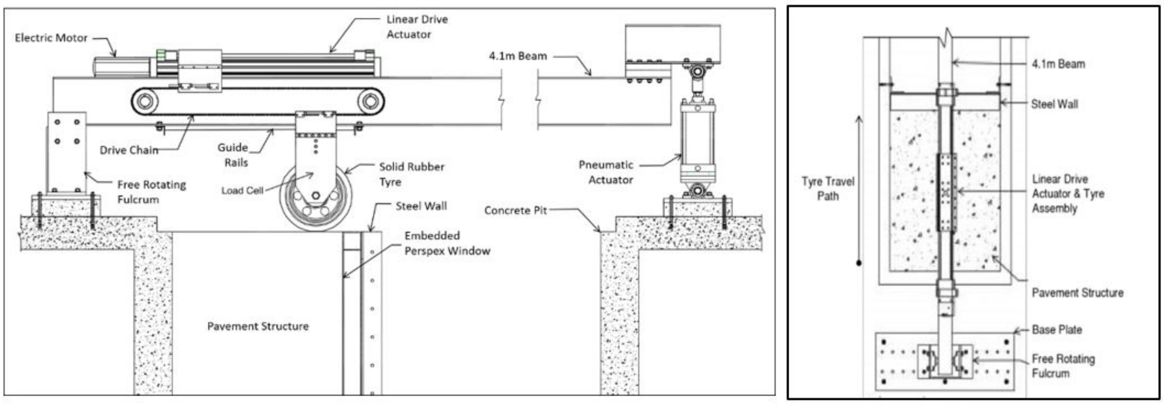

Figure 14: Side view and plan view of APT

An Accelerated Pavement Tester (APT) allowed controlled load to be applied onto the pavement through a single tyre. The pavement response and performance were monitored by a variety of on-apparatus and in-situ instrumentation. The APT differed from other accelerated pavement testers in that the Perspex window allowed the cross-section of the pavement to be seen clearly.

Figure 15: Image of APT

For loading of the tyre, the out-stroke of a pneumatic cylinder lifted the tyre out of contact with the pavement surface while the in-stroke provided the compression at the wheel/pavement interface. As the tyre position and height changed with each pass, the pneumatic actuator must apply a constant load to the pavement surface. The speed, position and load were controlled electronically via a fully automated digital control system. The actuator applied a pressure and the tyre side plate strain gauges measured the associated bending load from the tyre and digitally feedback to the control system, which adjusted the pressure in the pneumatic cylinder until the user input calibrated load was achieved. A feedback loop completed this cycle every 0.5 seconds. When the user-defined load was reached, the motor drive was initialized, moving the tyre forward. The loop continued to adjust the pressure through the entire cycle, ensuring a constant load was applied to the surface through the entire travel path. At the end, the load was released and the wheel assembly was moved back to its starting position. The process was repeated until a user-defined number of cycles or failure criterion was met (Bowman & Haigh, 2016).

The DASYLab (Data Acquisition System Laboratory) software offered real-time acquisition, analysis and control. The data acquired from the APT were collected in blocks and later combined in post-processing.

3.6 Boundary effects

The boundary effects caused by friction between the concrete tank wall and the soil could influence the movement and stresses of the granular material. To reduce the boundary effects, the wall interface was lined with a combination of plastic sheeting, silicon grease, geomembrane and geosynthetic. Similar methods have found a reduction in shear stress of 80% to 98% (Tawfiq & Caliendo 1993).

3.7 Water pump

Rainwater seepage can be modelled by injecting the water into the soil at a constant rate. In this project, water was introduced into the soil through a flexible tube connected to a peristaltic water pump. If the base course was present, the tube was placed in between the base course and the subgrade. Without the base course, the tube was placed on the surface of the subgrade. The water outflow rate was controlled by varying the pump speed. The position of the tube was marked on the window for result analysis purpose.

3.8 Particle Image Velocimetry (PIV)

A deformation measurement system based on Particle Image Velocimetry (PIV) which was originally developed in the field of fluid mechanics has been developed for use in geotechnical testing. PIV allows the movement of sand particles to be analysed by measuring displacement between pairs of images.

GeoPIV-RG is a MATLAB module which implements PIV for geotechnical and structural engineering research applications. It is an update of the GeoPIV program which represents the typical algorithm used in current research and is described in detail by White et al. (2003).

Figure 16 shows the basic principles of PIV analysis. PIV first divides the initial image (image 1) into a mesh of test patches. The correlation between each patch in image 1 and a larger patch from the same part of a subsequent image (image 2) is evaluated. The location at which the highest correlation is found indicates the position of the displaced patch. Once the operation for the entire mesh is done, the complete displacement of each test patch can be produced. (White & Take, 2002)

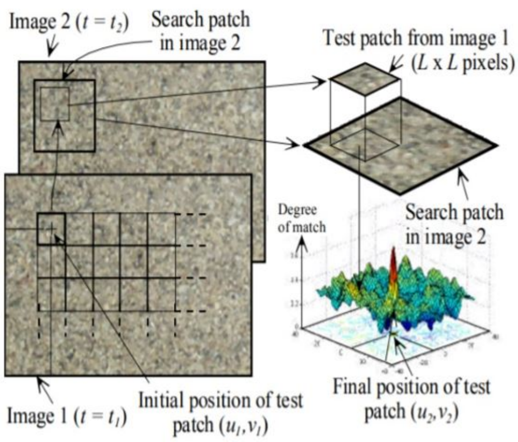

Figure 16: Basic principles of PIV (White & Take, 2002)

To provide a comprehensive analysis of the impact of the 'micro' view on subset texture quality, two subset texture quality parameters have been calculated: (i) the standard deviation of subset pixel intensities σ_{Is} (Stanier & White, 2013); and (ii) the sum of square of subset intensity gradients (SSSIG) (Pan et al., 2008). The former is a simple measure of the contrast within the subset with values of $\sigma_{Is} > 15$ indicating adequate contrast (Stanier & White, 2013). The latter is a measure of the distribution of the contrast with values of SSSIG $> 10^5$ indicating adequate texture distribution (Pan et al., 2008). The suitable subset quality measures $\sigma_{Is} > 15$ and SSSIG $> 1 \times 10^5$ are recommended for the analysis of high-resolution images. To improve accuracy of result, smaller subsets are used but the time taken to run the analysis will be longer. Therefore, a trade-off between time and quality is necessary.

In this project, the size of subset used was 50×50 px. The quality of the subsets based on the images captured is shown in Figure 17 below. This indicates that the image being analysed was of acceptable quality as most subset had a σ_{Is} greater than 15 and a SSSIG greater than 1×10^5.

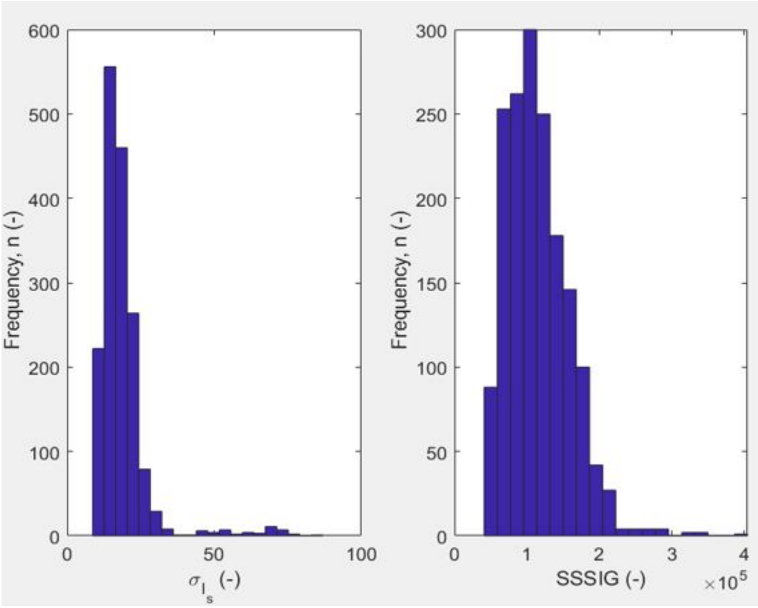

Figure 17: Quality of subsets

Using GeoPIV-RG, rigid-body displacements can be detected to a precision of ~ 0.001 px, irrespective of the rotation magnitude, whilst the mean errors are always less than 1×10^{-4} px (Stanier, et al., 2016).

4 RESULTS AND ANALYSIS

4.1 Test overview

Three test profiles were investigated in this project. The test profiles are shown in Figure 18 and the tests performed are summarised in Table 2 below.

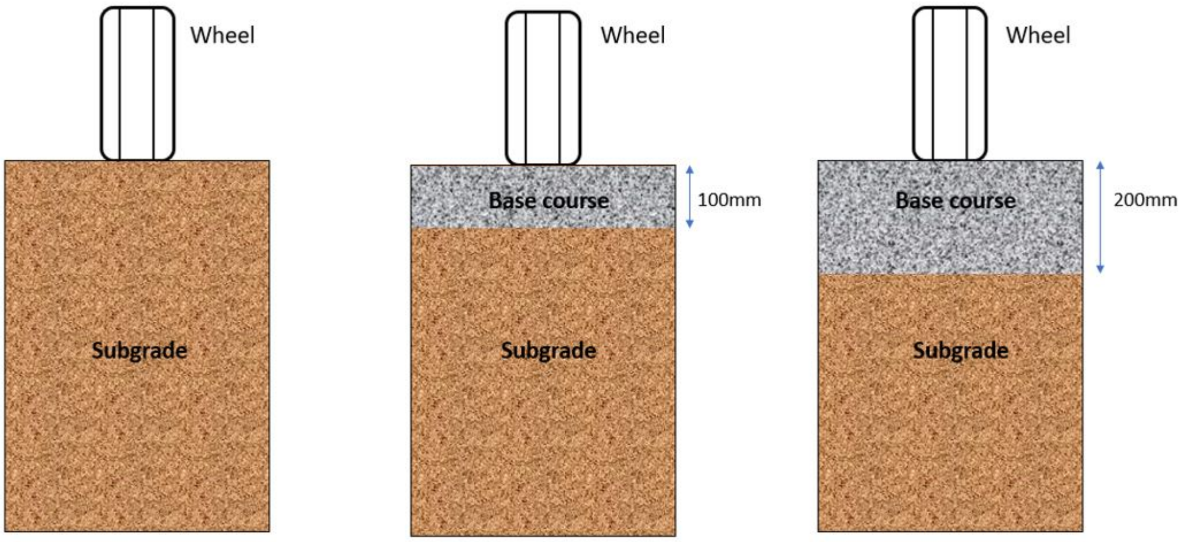

Figure 18: Test profiles

Table 2: Summary of tests performed

Test	Structural layers	Surface load, P(kN)	Number of cycles, n	Speed of wheel, v(mm/s)
1A	Subgrade	2.7	2	5.1
2A	Subgrade, 100 mm base course	3.7	300	25.6
3A	Subgrade, 200 mm base course	3.7	50	25.6
3B	Subgrade, 200 mm base course	4.7	60	25.6

4.2 Expansion of wet region in subgrade

4.2.1 Variation of displacement with distance from water source

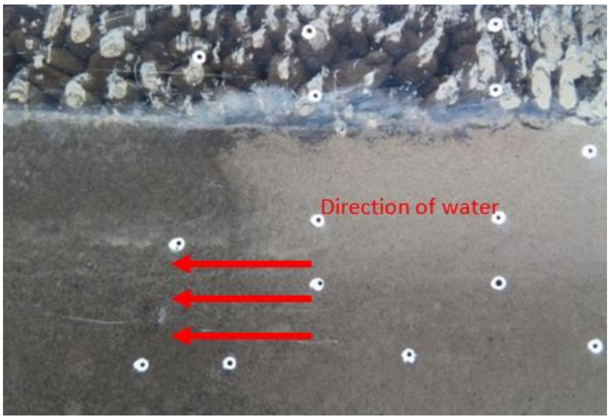

Figure 19: Direction of expansion of water edge

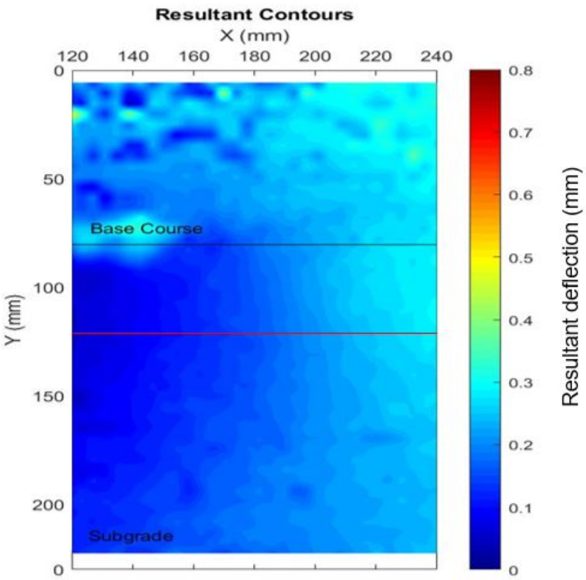

Figure 20: PIV indicating change in resultant deformation of subgrade in the direction of water expanding

The test was carried out on a 200 mm thick base course at a volumetric flow rate, Q of 10.3 ml/min. As the water front progressed from right to left (Figure 19), the subgrade strength weakened progressively as shown by the contours in Figure 20, which indicated a higher deflection nearer to the source of water. The deformation in the base course was also observed to be higher in the region closer to the water source. It is important to note that the stipples seen in the base course could be due to the immobile silts that were stuck onto the window, causing the PIV not being able to track the actual deformation in the base course.

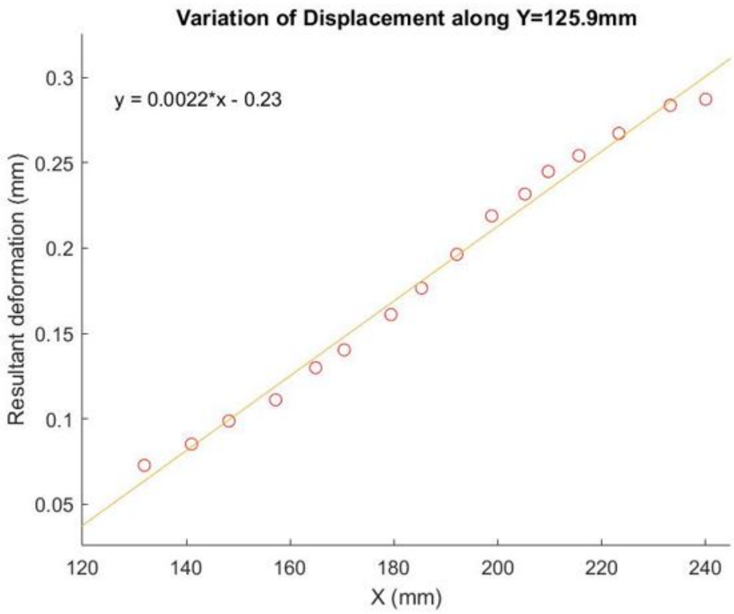

Figure 21: Variation of resultant displacement along Y=125.9 mm

Figure 21 shows the linear variation of displacement along Y=125.9 mm (Y was chosen randomly within the subgrade layer, marked by the red line in Figure 20). The further away the subgrade from the water source was, the smaller the displacement in the subgrade as the sand experienced loss of particles interlock and strength. This explains why when a crack is formed in the surface of an actual pavement and water infiltrates it, the subgrade beneath the crack starts to weaken progressively as the moisture content increases, which widens the crack and eventually leads to the formation of a pothole.

4.2.2 Rate of change of radius of wet zone

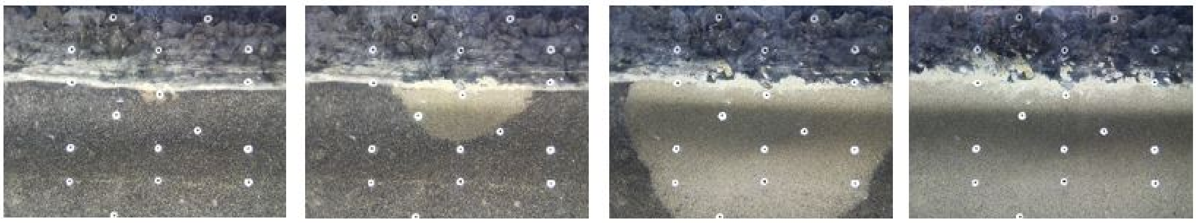

Figure 22: Edge of water expanding

Figure 22 shows the wet region expanding over time as seen from the images captured by one of the cameras. Figure 23 shows the plots for the rate of change of radius of wet zone, R for Q=3.47 ml/min and 10.3 ml/min. Both lines in the plot show that R increased linearly with time for both Q values.

The ratio between Q=10.3 ml/min and Q=3.47 ml/min was $\frac{10.3}{3.47} = 2.97$.

When Q increased by a factor of 2.97, the rate of change of R increased by a factor of $\frac{0.0057}{0.0029} = 1.97$.

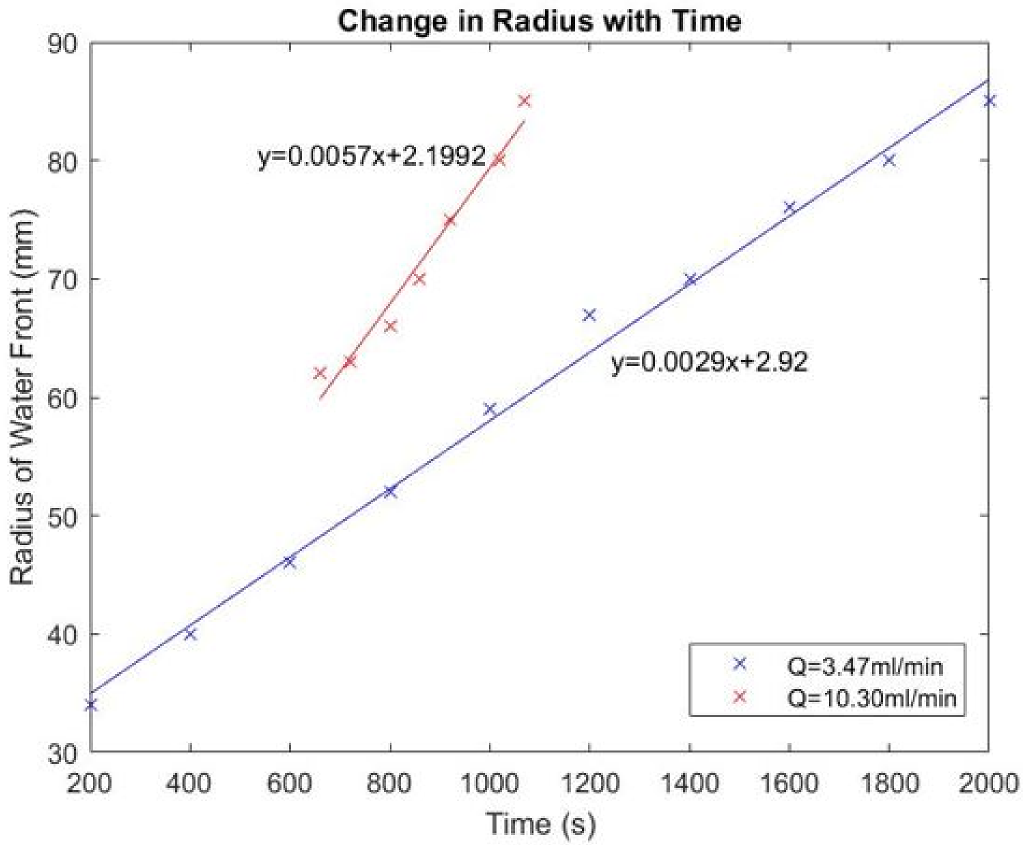

Figure 23: Change in radius R against time

When compared to an actual pavement, there will be a discrepancy in the rate of change of R. In the tests performed, water was unable to penetrate the Perspex window and was forced to move in other directions, which resulted in faster expansion of water edge. Without the window acting as an obstacle, water can move freely in all directions and the expansion of the water edge will be slower. Therefore, the displacement in the deeper layers of an actual pavement is expected to be lower.

4.3 Subgrade response without base course

4.3.1 Comparison between dry and wet subgrades

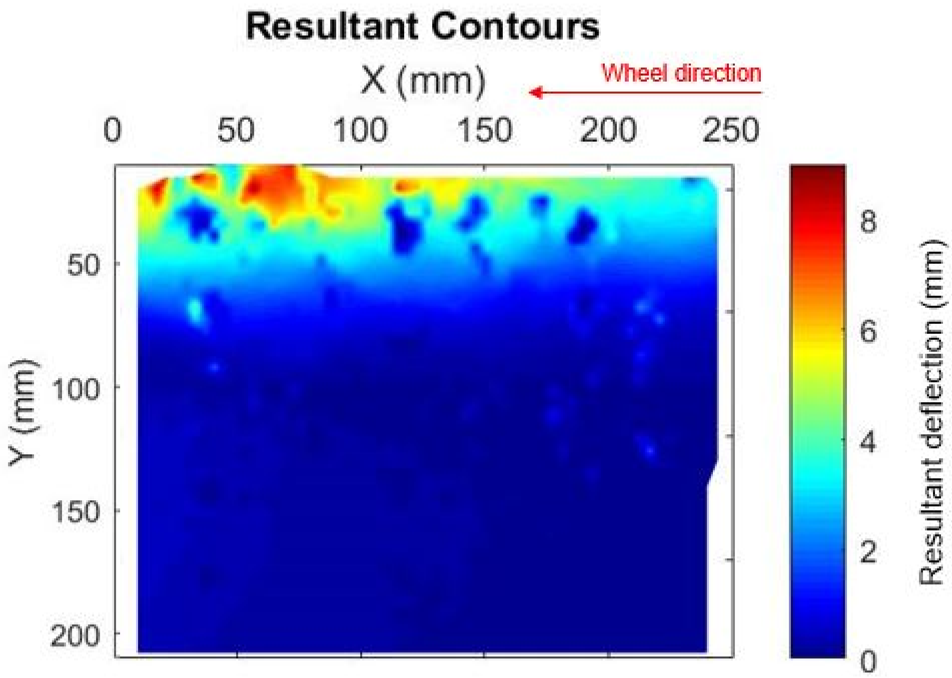

Figure 24: Resultant deflection of dry subgrade at P=3.7 kN

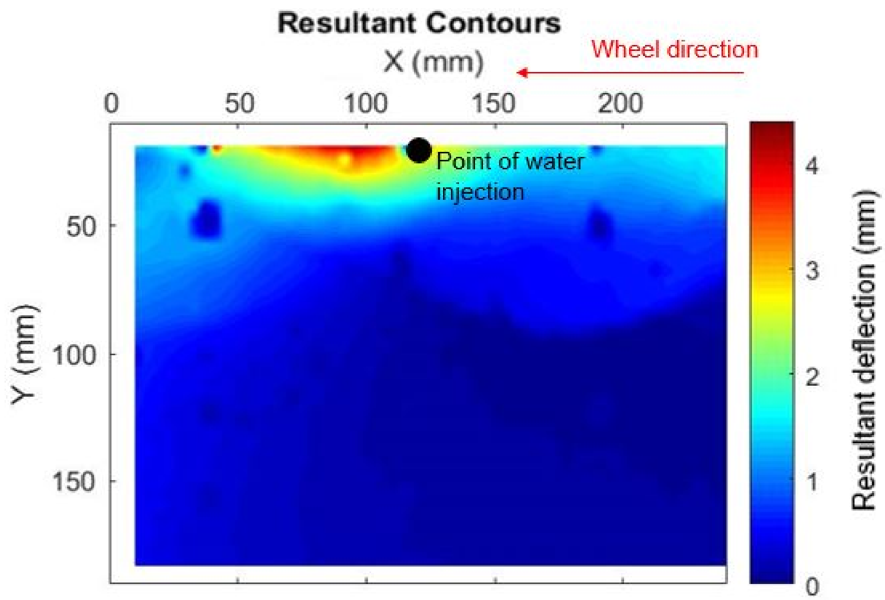

Figure 25: Resultant deflection of wet subgrade at P=2.7 kN

Figure 24 and Figure 25 show the cumulative resultant displacement of the subgrade under dry and wet conditions respectively after one wheel pass. In this project, dry subgrade refers to subgrade at the optimum moisture content and no additional water was introduced. Note that apart from a higher applied load, the resultant deformation in the dry subgrade was much higher than the wet subgrade due to the fact that multiple tests were first carried out on the dry subgrade (before adding water), which further compacted the soil. The speed of the APT tyre was only 5.1 mm/s as the subgrade was very weak and experienced larger deformation. The low tyre speed allowed more images to be captured in one cycle to provide better accuracy of results.

From the PIV analysis, the resultant displacement in the dry subgrade decreased linearly with depth and was approximately constant along the horizontal plane. With the wet subgrade, the resultant displacement was not constant horizontally and was non-linear with depth. A pothole was formed on the surface of the wet subgrade based on eye observation, and was also shown in the PIV analysis. The region where the displacement was the highest (red region shown in Figure 25) was where the pothole formed.

Figure 26: Pothole forming after 2 cycles on wet subgrade

Figure 26 above shows the development of a pothole forming after 2 wheel passes. Water was introduced at the centre of the pavement which can be seen from Figure 26 as well (wet sand has a darker shade than the dry sand). At the first pass, rutting could be observed as the subgrade experienced permanent deformation. As the wheel rolled over the subgrade, the water on the surface was squeezed and pushed forward and affected a bigger area of subgrade, which accelerated the subgrade failure. This explains why the deformation of the subgrade was bigger in front of the wheel and smaller at the back of the wheel based on PIV results. By the second pass, a large patch of the wet sand could be seen stuck onto the wheel and it was evident that the subgrade has failed. Without the base course, the wet surface of the unbound subgrade layer got carried away easily by the moving tyre. This situation did not occur with the dry subgrade, where only rutting was observed.

4.3.2 Vertical displacement in subgrade

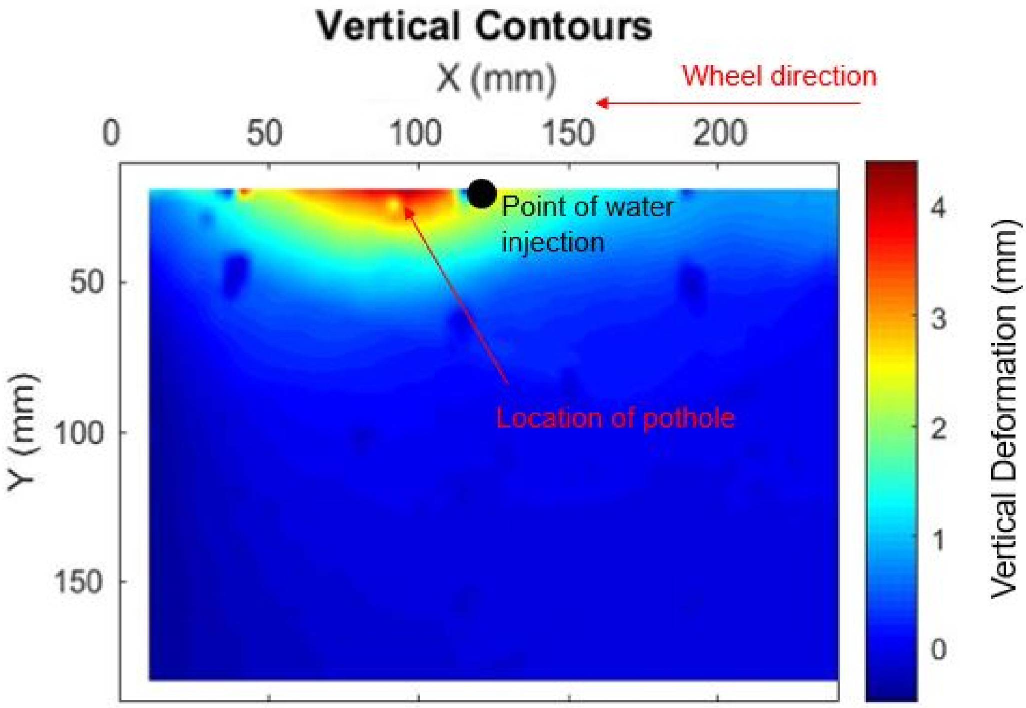

Figure 27: Vertical deflection of Test 1A

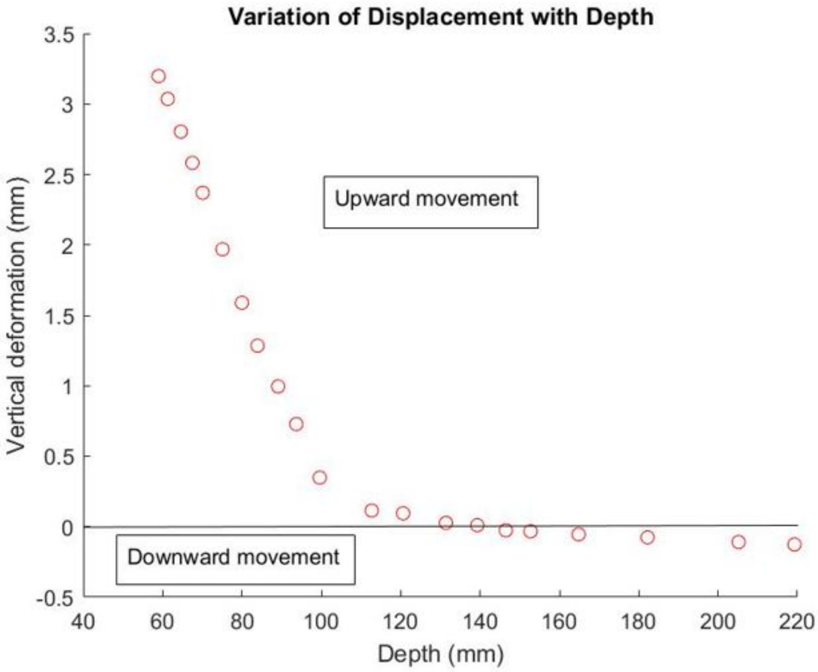

Figure 28: Variation of displacement with depth at the centre of pothole

Based on the observation of the surface layer, water had a huge impact on the permanent deformation of the surface layer but there was less impact on the lower layer of the subgrade. As sand drained very quickly, the change of saturation in the deeper layer was small and the loss of stiffness was less significant. The contours of vertical deflection of the subgrade are shown in Figure 27. Figure 28 shows the magnitude of vertical deformation decreasing with depth for Test 1A (2.7 kN) along the line at the centre of the pothole. The centre of the pothole was about 25 mm to the left of the point of water injection due to water being pushed forward by the moving tyre. Between depths of 0 and 140 mm, the vertical deflection on the side of the wheel was linear and upwards and beyond that the vertical deflection was downwards. Negative vertical deflection indicates downward displacement while positive indicates upward displacement.

Test 1A showed the influence of water at a single point of injection in the subgrade. When unpaved roads such as dirt roads encounter rainy weather, the rainfall is usually uniform over the whole surface. In this case, water infiltration would be uniform overall and the displacement expected would be constant along the surface, similar to the deformation behaviour demonstrated by the dry subgrade.

4.3.3 Upheaval of soil

In Bowman & Haigh's (2018) study, dilation was seen in the passive region on either side of the tyre which caused upheaval on both sides in the surface deformation. A rutting simulation was done by Wang et al. (2017) using finite element analysis and it also indicated upheaval on either side of the wheel with maximum downward vertical displacement in the centre of the wheel (Figure 29). Both tests considered Poisson's ratio, $\nu = 0.35$ to 0.45 for all pavement layers and were carried out based on the plane of symmetry perpendicular to the wheel.

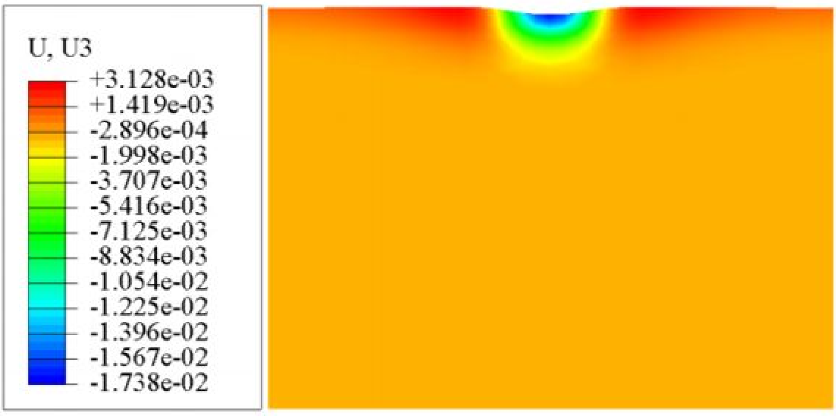

Figure 29: Rutting simulation result of feature section under wheel load of a wheel, units in cm (Wang, et al., 2017)

Upheaval was observed along the pavement as the wheel moved and appeared to be greater in the region of wet sand as ruts developed. The heaving seen was a result of rotational stress in the soil below the wheel. The major principal stress was vertical under the wheel while the major principal stress was horizontal beside the wheel. These active and passive regions were linked by a stress fan as shown in Figure 30.

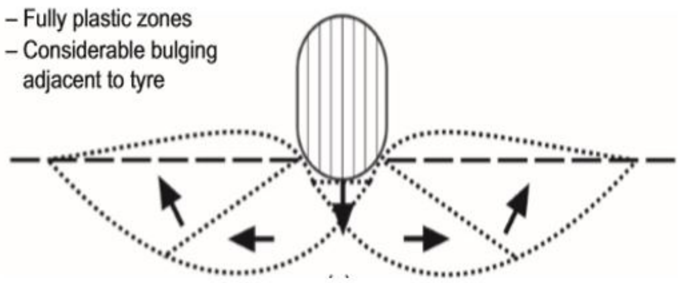

Figure 30: Front view of failure mechanism beneath a single tyre (Bowman & Haigh, 2018)

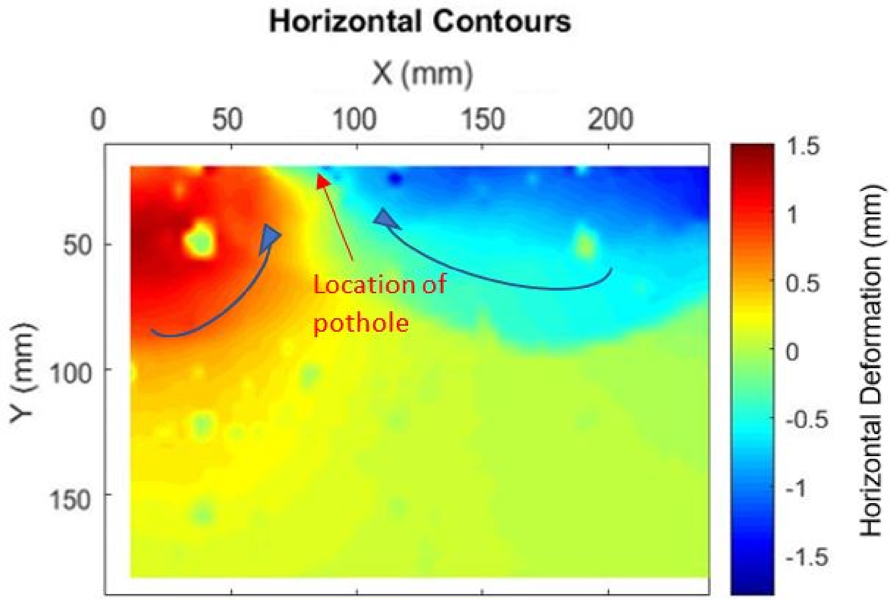

Figure 31: Horizontal deflection of Test 1A

The horizontal contours in Figure 31 showed the cumulative horizontal displacement of soil towards the centre of the pothole formed after 1 wheel pass. The negative sign of horizontal deflection indicates the movement of sand to the right while the positive sign indicates sand movement to the left. From the camera images, it was observed that as the tyre moved forward, the subgrade in front of the tyre was pushed forward while a small amount of subgrade behind the tyre was pushed backward, both in an upheaval manner. This justifies the upward vertical displacement and the horizontal displacement observed from the PIV at shallower depths. Figure 32 shows the upheaval beside the wheel.

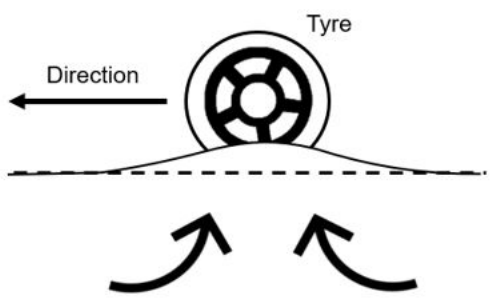

Figure 32: Side view of upheaval beside a single tyre

4.3.4 Shear strains in subgrade

Figures 33 and 34 show the shear strain, γ and volumetric shear strain, ϵ_v for Test 1A. Positive strains are compressive while negative strains are dilative. For both strains, the magnitude was the highest at the region where large deformation was observed, which was where the pothole formed. The strains were localized around the region beneath the pothole and they decreased with depth. The volumetric strain showed dilation as a result of upheaval in the soil beside the tyre.

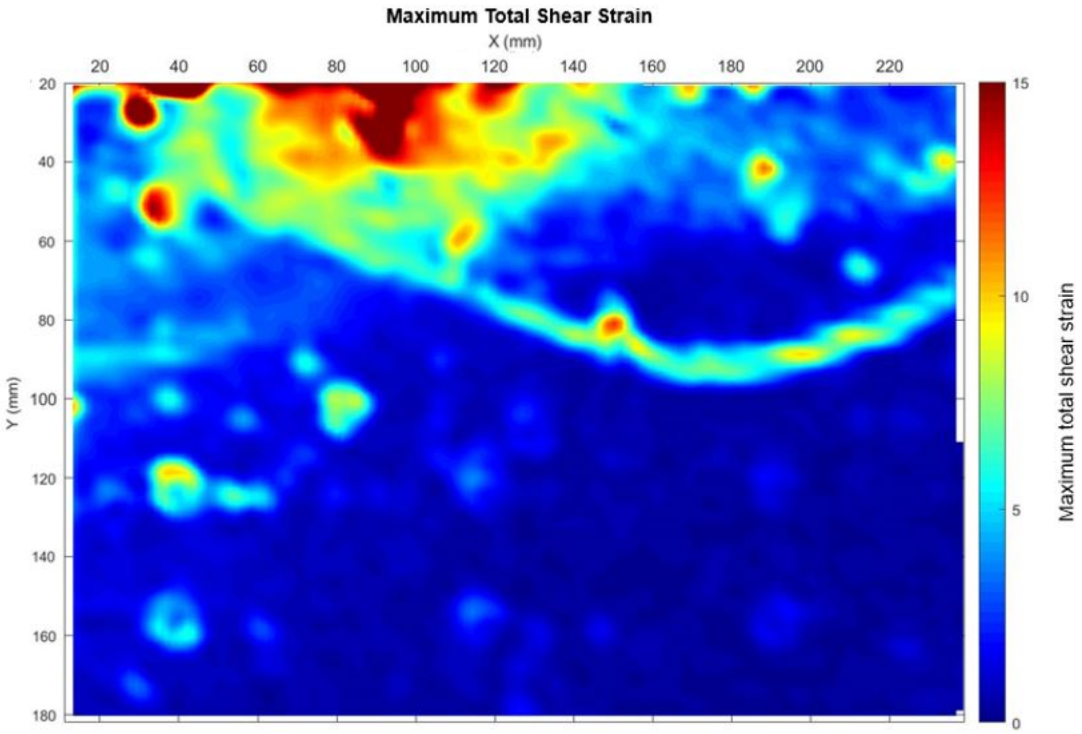

Figure 33: Maximum shear strain for Test 1A

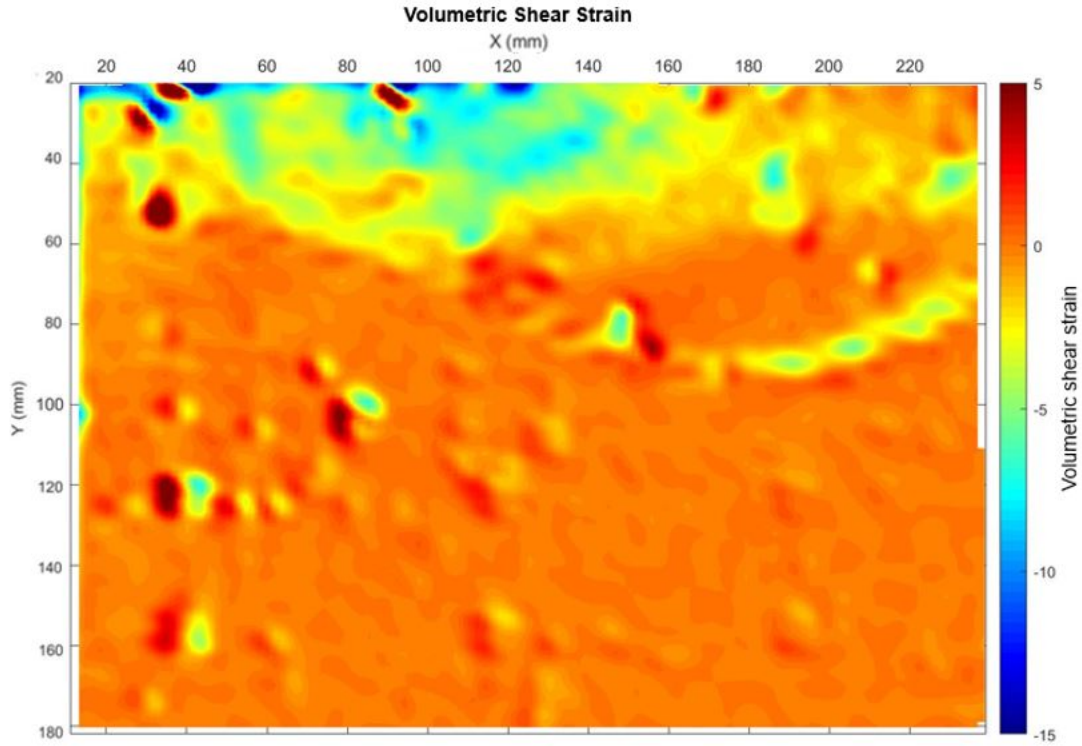

Figure 34: Volumetric shear strain for Test 1A

4.3.5 Layer-elastic analysis

Burmister's layer-elastic theory was applied to predict the vertical displacement at 11.1% optimum and 21% water contents. An increase in water content will reduce the resilient modulus of the pavement layers. The Poisson's ratio, ν for the subgrade was 0.35 based on triaxial test results. Burmister's theory was based on a stationary load with a circular contact. The contact area between the wheel and the pavement varies depending on the wheel load applied and the relationship is shown in Figure 35. Figure 36 shows the variation of vertical displacement with depth based on Burmister's solutions for a load of 2.7 kN. The width of tyre was 236 mm.

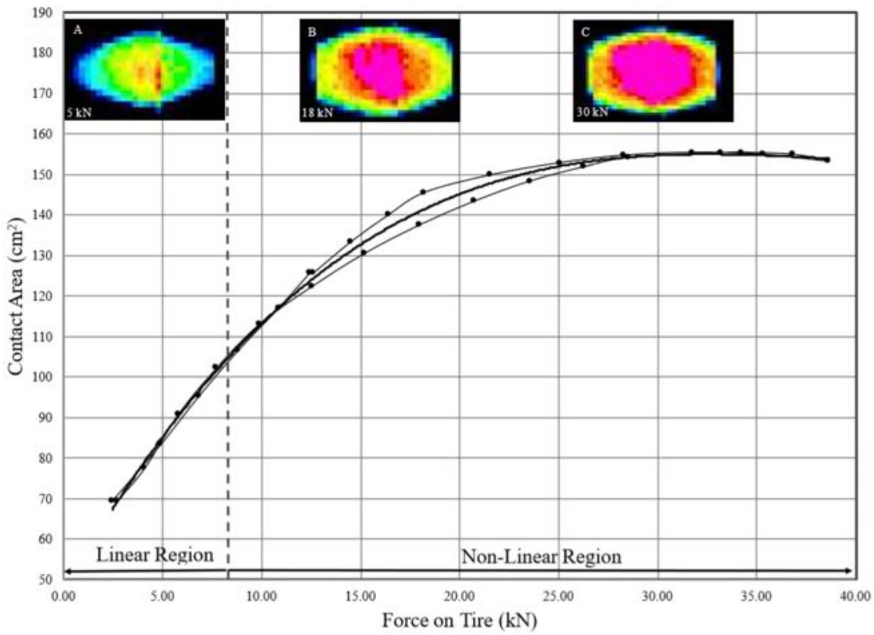

Figure 35: Contact area of APT tyre due to load including pressure distribution at various loads from Tekscan data

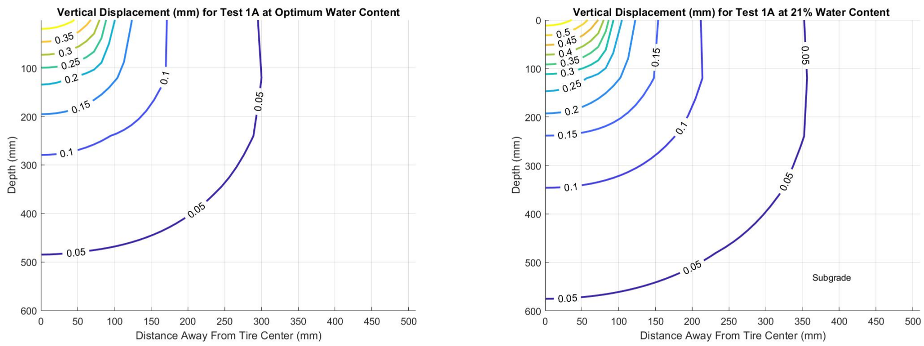

(a) Optimum water content (b) 21% water content

Figure 36: Vertical displacement for Test 1A

The layer-elastic solutions (Figure 36) did not capture the upheaval that occurred under the wheel load. At depths 0 to 100 mm, the solutions were much less than the actual displacement obtained from PIV analysis (Figure 28), even for solutions at a higher water content (21%). However, at deeper depths when the water content was closer to the optimum, the actual result was closer to Burmister's result. For instance, at a depth of 200 mm, the predicted displacement was 0.15 mm while the actual result was 0.11 mm, but the percentage difference was still 27%, which is very high. Therefore, under a moving wheel load, Burmister's solution may not be an accurate representation of the actual result in this case, as there was a cumulative displacement and strain in the subgrade as the wheel moved along the surface. The upheaval in the subgrade was also not accounted for in Burmister's solution.

4.4 Subgrade response with base course

4.4.1 Development of deformation in base course and subgrade

Water being injected into the subgrade at the base course/subgrade interface is similar to modelling water infiltration through a crack in the layers above the subgrade in an actual pavement. For test profile 2A with 100 mm base course, water was introduced at a rate of 3.53 ml/min into the subgrade. PIV analysis was carried out to analyse the displacement in the subgrade layer. Figures 37, 38 and 39 show the PIV results for the resultant displacement of the layers. The load of 3.7 kN was chosen to model the weight of a normal car (4 wheels) that is approximately 15 kN, which gives a single tyre load of about 3.7 kN.

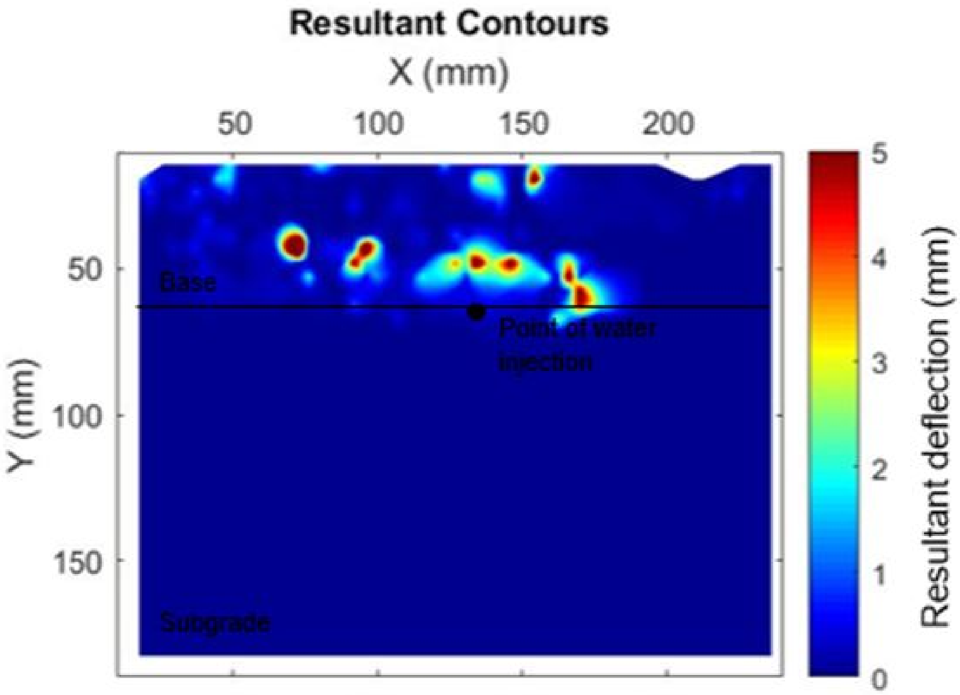

Figure 37: Resultant displacement for 1-20th cycle

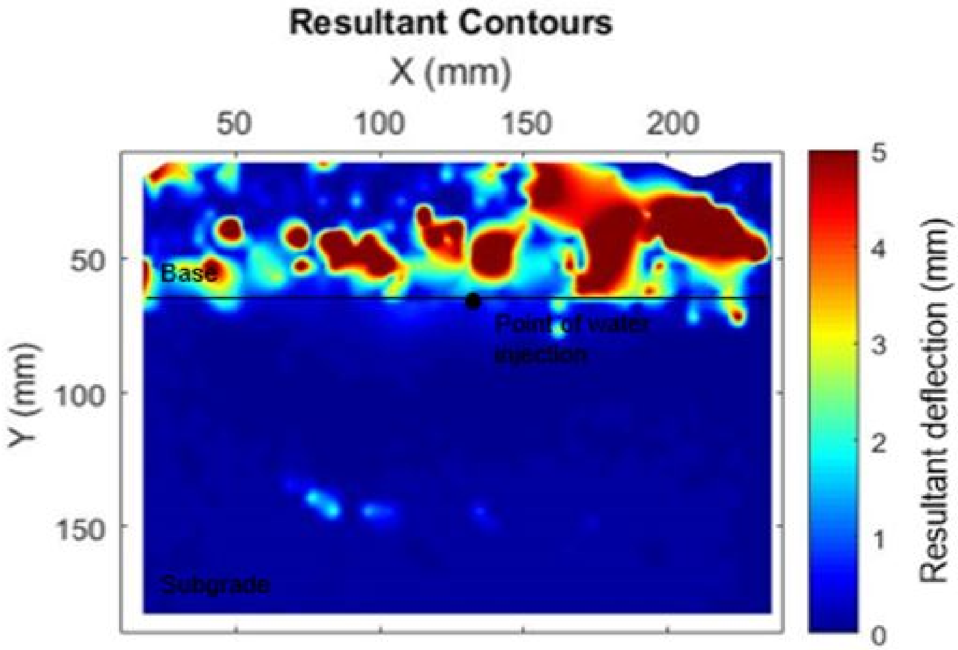

Figure 38: Resultant displacement for 1-100th cycle

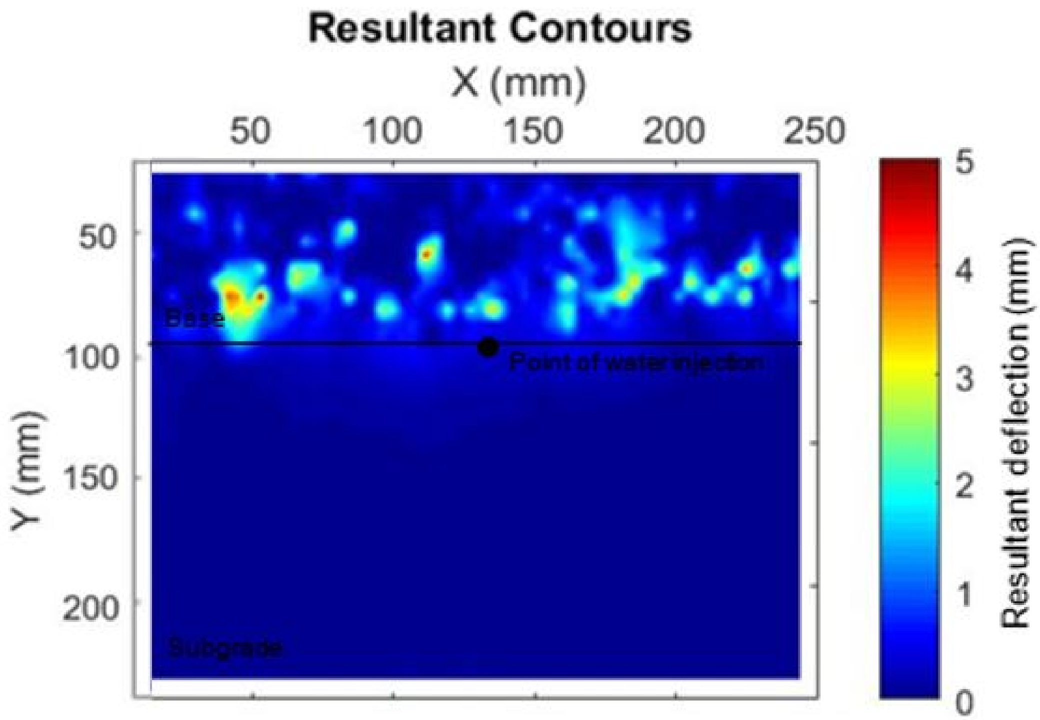

Figure 39: Resultant displacement for 100-300th cycle

In the first 100 cycles, large displacements were observed in the base course. This was due to the collapse of voids in the base course as the wheel rolled over the layer. This load caused further compaction to the base course layer. From the series of images captured, it was also observed that some of the limestone aggregates were crushed, which created more voids, leading to more voids collapsing. The crushed fines then filled up other voids in the base course. At this point, the area of wet subgrade was still small. There was little displacement in the subgrade layer. Dawson & Kolisoja (2004) observed that there was a loss of strength when the fines content became excessive. At higher fines content, the coarser aggregate (base course) was 'floating' in a matrix of finer particles. This reduced the contact points of the aggregates which resulted in loss of strength.

As the wet region expanded and load reptition increased, the area of subgrade affected by the water underwent bigger displacement than the unaffected area over time. Larger displacement was observed in the centre of the subgrade, where water was being injected into. Apart from crushing of the limestone aggregates, the images also showed capillary action in the base course. Water was being sucked up from the subgrade into the voids of the base course. This action caused the fine silts being 'washed out' of the voids of the limestone aggregates, which increased the void size as a result, and eventually led to weakening of the base course. If water fills in all the voids between the aggregate particles (non-draining condition) the pore water may be pressurised under wheel loading. The water pressure can counteract the particle contact stresses, which will result in considerable reduction in the material strength.

When the subgrade became more saturated with water (at 100 cycles and above), displacement occurred across the layer of the subgrade. This strongly supports the fact that moisture ingress causes the weakening of the subgrade, which accelerates the failure of pavement.

For the 200 mm base course, water was injected into the base course at a rate of 10.3 ml/min. Initially, the APT was running at an applied load of 3.7 kN for the first 50 cycles. After that, the applied load was increased to 4.7 kN and was left to run for the next 60 cycles.

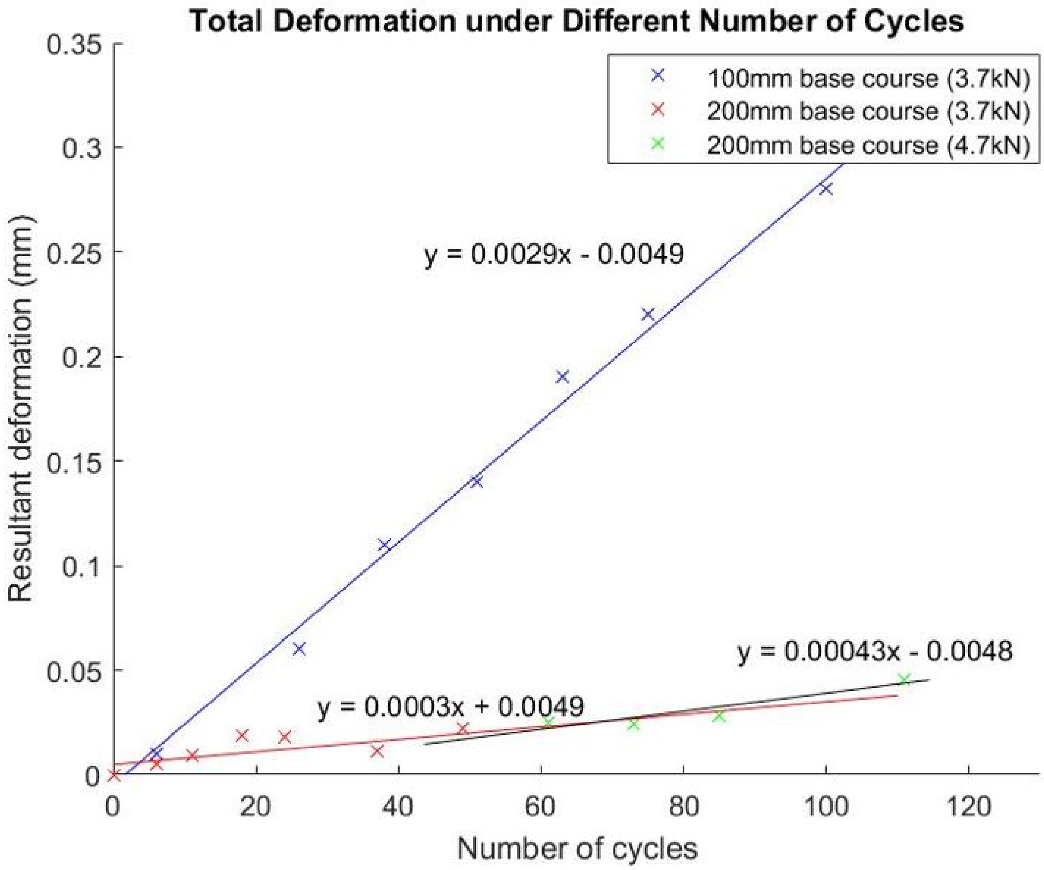

Figure 40: Resultant deformation of subgrade with increasing number of cycles

Based on Figure 40, the total deformation increased linearly with number of cycles at a constant load. There was an increase in gradient of the line from 0.0003 mm/cycle to 0.00043 mm/cycle (factor of 1.4) as the load increased from 3.7 kN to 4.7 kN (factor of 1.3). This suggests another possible linear relationship between load and deformation. However, more loads should be tested out to verify this linear relationship.

4.4.2 Comparison with subgrade without base course

The base course has an elastic Young's modulus, E of 19.33 MPa while subgrade has an E of 13.16 MPa. Therefore, the base course can withstand greater loads and number of load cycles before failing. From the tests carried out, the base course did not fail even after 300 cycles and the deflection in the subgrade layer was much smaller in comparison to the test without base course. On the other hand, without the base course, the subgrade failed after one or two cycles under the influence of water. Besides acting as a load-bearing layer, the base course also helped to hold the unbound layer of subgrade in place which prevented the soil from being carried away by the moving wheel.

4.5 Influence of thickness of base course on subgrade response

4.5.1 Deformation in 100 mm & 200 mm base course

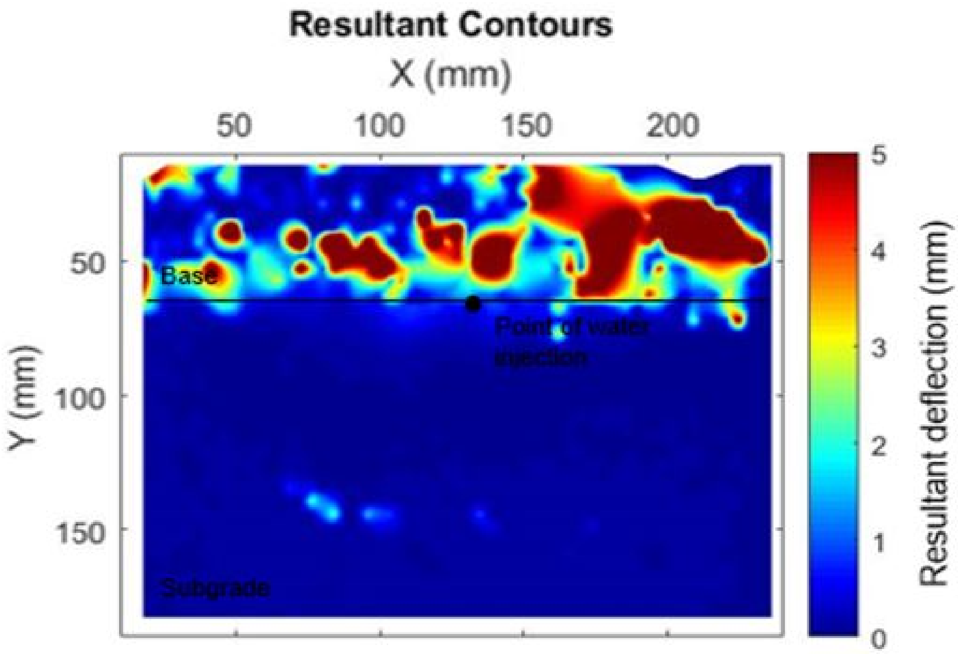

Figure 41: Resultant displacement for 100 mm base course

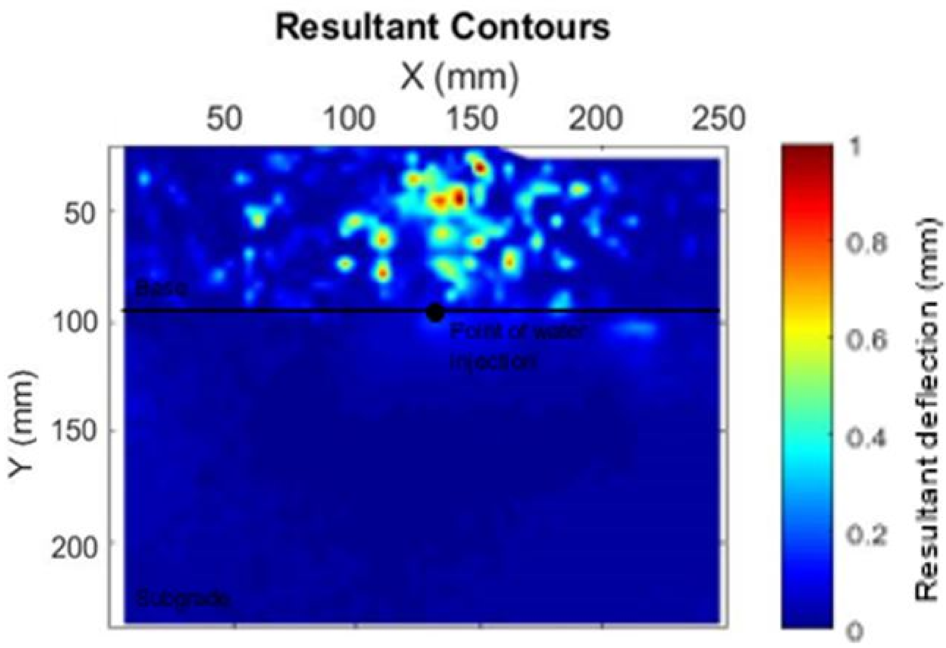

Figure 42: Resultant displacement for 200 mm base course

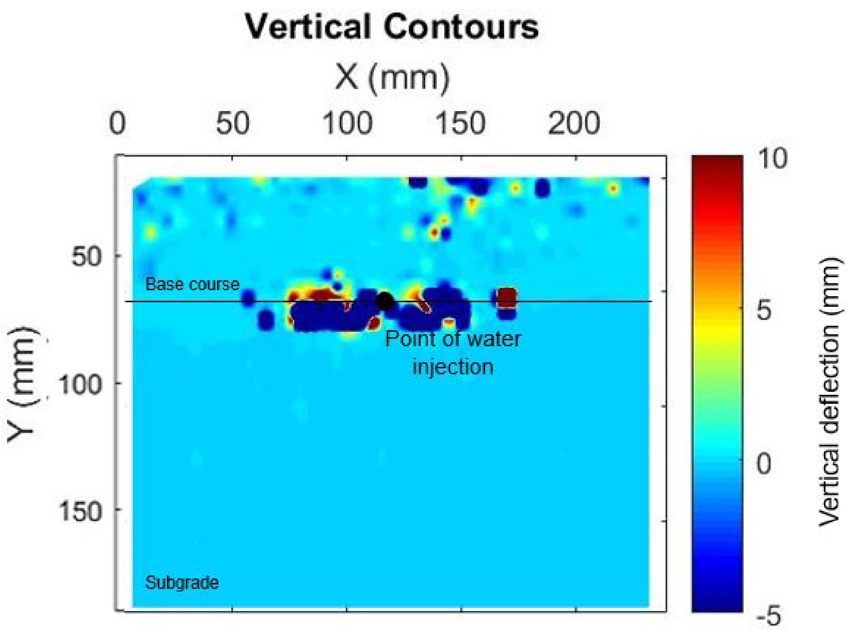

Figure 43: Vertical displacement for 100 mm base course

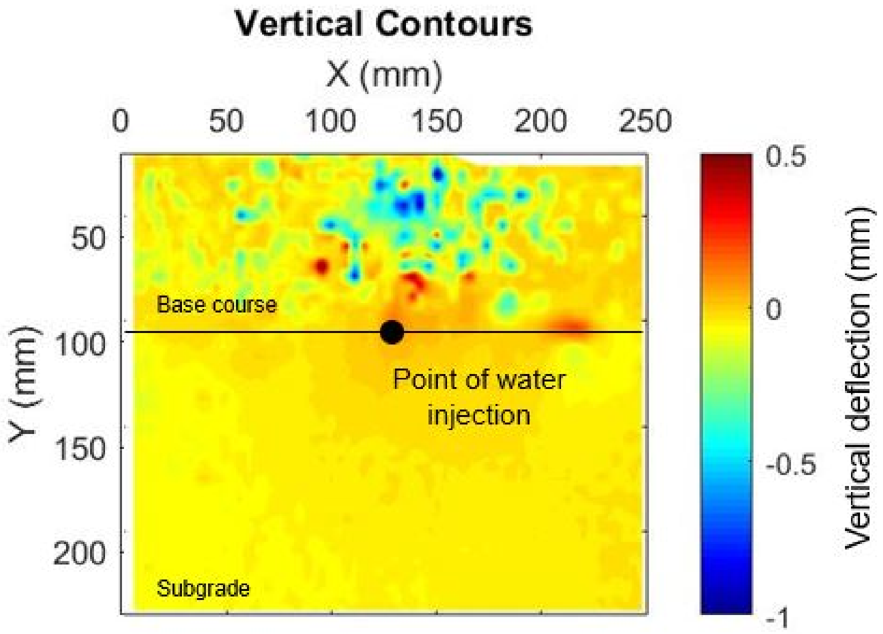

Figure 44: Vertical displacement for 200 mm base course

Figures 41 to 44 showed the cumulative resultant and vertical displacements after 100 cycles for 100 mm and 200 mm thick base course. For the 100 mm base course, the images for PIV analysis were taken by the top camera while for the 200 mm base course, the images were taken by the bottom camera. The maximum vertical displacement at the point of water injection in the subgrade with a 100 mm base course was around 0.10 mm, while the maximum vertical displacement in the subgrade with a 200 mm base course was only about 0.015 mm despite having a higher volumetric flow rate. With the 100 mm base course, the resultant contours show that the deformation was more spread out with larger displacement in the subgrade at the point of injection of water, indicating a more flexible pavement compared to the 200 mm base course. Displacement in the base course was also observed to be spread out across the layer.

On the other hand, the 200 mm base course showed a more localised displacement in the subgrade around the point of water injection. This is because thicker pavement structures exhibit less sensitivity to moisture content variations due to the fact that lower stress levels are experienced by the subgrade (Huang, 2003). The results also agreed with Bowman & Haigh (2018), whereby reducing the structural layer's thickness results in increasing vertical deflection, which penetrates deeper into the pavement. In the base course, the displacement was also more localised to the area above the point of water injection. This shows that the weakening of subgrade layer subsequently weakens the base course above it.

4.5.2 Layer-elastic analysis

Figure 45 to Figure 46 show the difference in vertical displacement between 100 mm and 200 mm thick base course by applying Burmister's layer-elastic theory at two different water contents.

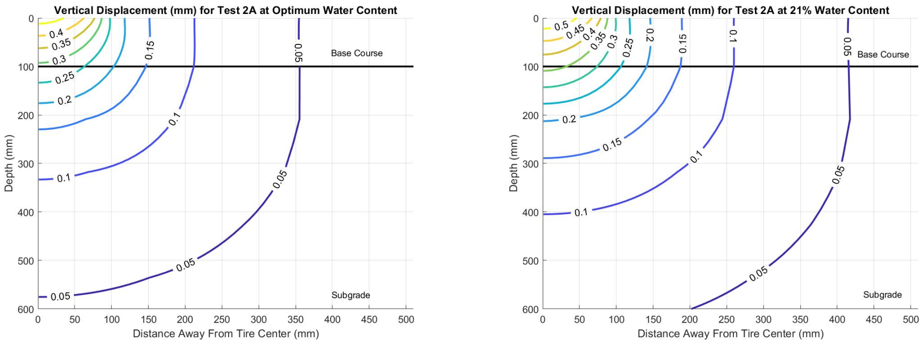

(a) Optimum water content (b) 21% water content

Figure 45: Vertical displacement for Test 2A

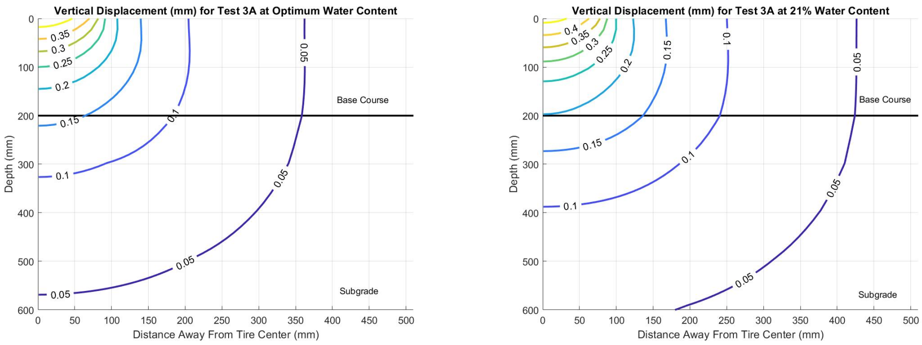

(a) Optimum water content (b) 21% water content

Figure 46: Vertical displacement for Test 3A

Unlike Test 1A where the base course was absent, the base course in Test 2A and Test 3A prevented the upheaval of subgrade. There was a discrepancy between the actual and Burmister's results. For Test 2A, at a depth of 100 mm, the displacement based on layer-elastic analysis was 0.3 mm at optimum water content and 0.35 mm at 21% water content. For Test 3A, at a depth of 200 mm, the displacement based on layer-elastic anlaysis was 0.14 mm at optimum water content and 0.2 mm at 21% water content. The results were much higher than the actual displacement obtained, even though Test 2A and Test 3A had withstood many cycles of wheel pass. Apart from cumulative displacement and strain under a moving wheel load, one other possible explanation for this is that the actual moisture content in the subgrade was unknown as it changed over time which made it difficult to model the deformation using layer-elastic theory, since the resilient modulus also changed with varying moisture content. The displacement in the base course was also harder to track due to the silts sticking on the window.

5 CONCLUSIONS & FUTURE WORK

In wet regions, moisture content and temperature change have a significant impact on the mechanical behaviour of unbound materials in pavement. A considerable amount of studies have been conducted to study the impact of moisture variation on pavements. However, most of these studies have only focused on the asphalt surface layer rather than the weak subgrade.

Therefore, this project included the study of the effect of moisture on subgrade failure to better understand the deformation of the weakest layer in pavements. The transparent Perspex window allowed the cross-section of the pavement to be seen clearly, enabling a visualization of how subgrade deformation develops under repeated wheel loading. Images captured by the cameras were analysed with PIV to give the displacement and strain in the subgrade. Major findings from this study are as follows:

- The further away the subgrade is from the point of water infiltration, the smaller the displacement in the subgrade.
- Without the base course, subgrade alone is very much weaker. Water has a huge impact on the surface layer but there is less impact on the lower layer of the subgrade as sand drains quickly. The wet region of the subgrade where a pothole forms undergoes large displacements and strains. Upheaval of soil beside the wheel is larger in the wet region than in the dry region.
- Resultant deflection in subgrade increases linearly with the number of wheel passes. As the wheel load increases, the deflection at the point of water infiltration also increases.
- Capillary action at the interface between subgrade and base course further weakens the pavement as silts in the base course are washed away, increasing the void size in the base course.
- Thicker base course is less sensitive to moisture content variations, therefore it experiences less deformation than a thinner base course. With a thin base course, deformations in both subgrade and base course are more spread out. On the other

hand, deformation in the subgrade is more localised around the wet region when the base course is thicker, which subsequently leads to weakening of the base course above the wet region.

- Layer-elastic theory is not a suitable model to predict the change in deformation and stresses under a moving wheel load.

5.1 Recommendations for future work

When the base course (a mixture of silt and limestone aggregates) is mixed with water, the silt tends to stick to the surface of the Perspex window. The immobile silt causes difficulty in carrying out PIV analysis as the PIV only tracks the silt, resulting in displacement in the base course not being observed. For future research, it is worth considering methods such as lubricating the surface of the window, to prevent the silts from sticking onto it.

The areas of study in this project can be extended in several ways. Firstly, the tests conducted in the project only consisted of base course and subgrade to simplify analysis. In real life, pavements consist of more than just the two layers and it would be interesting to investigate the impact of water that can have on the different layers. It is also worth installing moisture sensors to measure the moisture content at different layers of soil, to enable study on the deformation and strain response of soil under different moisture content to be carried out.

Furthermore, geotextiles are widely used in road construction nowadays to improve the lifespan of roads. The four primary uses of geotextiles are separation, drainage, filtration and reinforcement. The effectiveness of having geotextiles can be studied to understand the effect it has on the deformation and response of the subgrade. The geotextile should be placed in between the base and subgrade and a comparison can be made with the result of the study without geotextiles.

In this project, the results obtained are only applicable for short-term response as the number of wheel passes of the APT was only up to a few hundred. To observe the long-term response of pavements, it may be the case where thousands or even hundred thousands of cycles are required (for instance, the study carried out by Wiman (2001) and Erlingsson (2010)) to obtain the pavement deformation, stress and strain behaviours.

Finally, the study conducted is only limited to one type of soil with specific properties. Cambridge and some other regions in the UK tend to have clayey soil. Since clay has different properties from sand, it most likely exhibits a different behaviour from sand in terms of response and stress dependency. Clay tends to demonstrate undrained behaviour in contrast to the Oxford sand used in this project which is closer to drained behaviour. As a result, clay can develop negative pore pressure while sand cannot. Pore pressure build-up may take place which can result in considerable bearing capacity loss. It is worth carrying out a similar study on clay to understand the performance of pavement with a different type of subgrade soil.

6 APPENDIX

Risk Assessment

The risks from the safety hazards that were listed in the Risk Assessment Form were minimised or avoided by taking appropriate control measures that are also listed in the form. A health and safety briefing was also conducted at Schofield Centre and it was compulsory for everyone who used the facilities there to attend. Another hazard that was identified during the course of the project but not listed in the Risk Assessment Form was toppling of the mixer. The mixer could be unstable at times and required support from toppling over when emptying the contents of the mixer into the pit. The risk of this happening was low, and the problem could be easily tackled by having another person holding the handles of the mixer when running it.

7 BIBLIOGRAPHY

Bowman, A. & Haigh, S., 2016. *The Cambridge Airfield Pavement Tester*, s.l.: 3rd European Conference on Physical Modelling in Geotechnics.

Bowman, A. J. & Haigh, S. K., 2018. *Subsurface deformation mechanisms beneath a flexible pavement using image correlation.* Géotechnique, pp. 1-11.

Burmister, D. M., 1958. *Evaluation of pavement systems of the Washo Road Test by layered system methods*, s.l.: The National Academies of Sciences, Engineering, and Medicine.

Dawson, A. & Kolisoja, P., 2004. *Permanent Deformation*, s.l.: Roadex II.

Ekblad, J. & Isacsson, U., 2006. *Influence of Water on Resilient Properties of Coarse Granular Materials.* Road Materials and Pavement Design, 7(3), pp. 369-404.

Erlingsson, S., 2010. *Impact of Water on the Response and Performance of a Pavement Structure in an Accelerated Test.* Road Materials and Pavement Design, Volume 11(4), pp. 863-880.

Foster, C. R. & Ahlvin, R. G., 1954. *Sresses and deflections induced by a uniform circular load*, s.l.: The National Academies of Sciences, Engineering, and Medicine.

Gaspard, K.,Zhang, Z., Gautreau, G., Hanifa, K., Zapata, C. E. & Abufarsakh, M., 2019. *Modeling the Resilient Modulus Variation of In Situ Soils due to Seasonal Moisture Content Variations.* Advances in Civil Engineering, 2019 (Article ID 1793601), p. 7.

Haynes, J. H. & Yoder, E. J., 1963. *Effects of Repeated Loading on Gravel and Crushed Stone Base Course Materials Used in the AASHO Road Test*, West Lafayette, Indiana: Joint Highway Research Project, Indiana Department of Transportation and Purdue University.

Huang, Y. H., 2003. *Pavement Analysis and Design.* 2nd ed, s.l.: Pearson Prentice Hall.

Leishman, F., 2019. *Cambridgeshire Live.* [Online] Available at: https://www.cambridge-news.co.uk/news/cambridge-news/cambridgeshire-pothole-nightmare-rac-council-15604099 [Accessed 3 January 2019].

Lekarp, F., Isacsson, U. & Dawson, A., 2000. *State of the Art. I: Resilient Response of Unbound Aggregates. Journal of Transportation Engineering*, 126(1), pp. 66-75.

Nazeri, A., Ziaie Moayed, R. & Ghiasinejad, H., 2018. *Effect of Base Coarse Layer on Load-Settlement Characteristics of Sandy Subgrade Using Plate Load Test.* International Journal of Geotechnical and Geological Engineering, 12(8), pp. 520-524.

Qiao, D., Dawson, A., Huvstig, A., Korkiala-Tanttu, L., 2014. *Calculating Rutting of Some Thin Flexible Pavements from Repeated Load Traixial Test Data.* International Journal of Pavements Engineering, 16(6), pp. 467-476

Saad, B., 2014. *Analysis of excess water impact on the structural performance of flexible pavements. International Journal of Pavement Engineering*, 15(5), pp. 409-426.

Saevarsdottir, T. & Erlingsson, S., 2013a. *Water Impact on the Behaviour of Flexible Pavement Structures in an Accelerated test.* Road Materials and Pavement Design, 14(2), pp. 256-277.

Saevarsdottir, T. and Erlingsson, S., 2013b. *Effect of Moisture Content on Pavement Behaviour in a Heavy Vehicle Simulator Test.* Road Materials and Pavement Design, 14(sup1), pp. 274-286.

Stanier, S., Blaber, J., Take, W. & White, D., 2016. *Improved image-based deformation measurement for geotechnical applications.* Canadian Geotechnical Journal, 53(5), pp. 727-739.

Wang, Y., Lu, Y., Si, C. D. & Sun, T., 2017. *Finite Element Analysis for Rutting Prediction of Asphalt Concrete Pavement under Moving Wheel Load.* International Journal of Simulation Modelling , 16(2), pp. 229-240.

White, D. & Take, W., 2002. *GeoPIV: Particle Image Velocimetry (PIV) sofware for use in geotechnical testing*, s.l.: Cambridge University Engineering Department.

Wiman, L. G., 2001. *Accelerated load testing of pavements: HVS-NORDIC tests in Sweden 1999*, S-581 95 Linköping Sweden: Swedish National Road and Transport Research Institute.